Food Chemistry: X 24 (2024) 101937

Contents lists available at ScienceDirect

Food Chemistry: X

journal homepage: www.sciencedirect.com/journal/food-chemistry-x

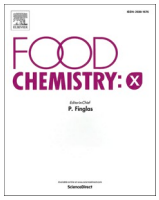

Comparative analysis of multifaceted properties of *Agaricus bisporus* and *Ganoderma lucidum* macro-fungi powder: Techno-functional and structural characterization, mineral uptake, and photocatalytic activity

Vaishali Singh [a], Aarti Bains [b], Gulden Goksen [c], Vittorio Capozzi [d], Anarase Dattatray Arjun [e], Nemat Ali [f], Muzaffar Iqbal [g], Prince Chawla [a,*]

[a] Department of Food Technology and Nutrition, School of Agriculture, Lovely Professional University, Phagwara 144411, India
[b] Department of Microbiology, Lovely Professional University, Phagwara 144411, India
[c] Department of Food Technology, Vocational School of Technical Sciences at Mersin Tarsus Organized Industrial Zone, Tarsus University, 33100 Mersin, Turkey
[d] Institute of Sciences of Food Production, National Research Council (CNR), c/o CS-DAT, Via Michele Protano, 71121 Foggia, Italy
[e] Directorate of Mushroom Research, Solan 173213, India
[f] Department of Pharmacology and Toxicology, College of Pharmacy, King Saud University, P.O. Box 2457, Riyadh 11451, Saudi Arabia
[g] Department of Pharmaceutical Chemistry, College of Pharmacy, King Saud University, Riyadh 11451, Saudi Arabia

ARTICLE INFO

Keywords:
Macro-fungi
Agaricus bisporus
Ganoderma lucidum
Bioactive compound
Polysaccharide
Antimicrobial
Photocatalyst
Dye degradation

ABSTRACT

Macro-fungi are recognized for food, medicinal, and environmental applications, therefore, the study focuses on multifaceted nutritional, techno-functional, and bioremediation-related uses of *Agaricus bisporus* and *Ganoderma lucidum* powders. Herein, *A. bisporus* exhibited 11.43 % significantly higher protein content, whereas, *G. lucidum* exhibited 63.55 % higher fiber content. For both mushrooms, spherical porous and fibrous interconnected structural morphology was observed, which led to distinguishing crystallinity and techno-functional properties. *G. lucidum* demonstrated 75.89 % higher iron, and 19.22 % higher zinc bioavailability while *A. bisporus* displayed 45.36 % higher calcium bioavailability. *G. lucidum* absorbed significantly higher zinc and calcium during cellular uptake, while *A. bisporus* revealed higher iron uptake. Both macro-fungi enhanced iron storage, with *G. lucidum* achieving 28.68 ± 0.61 ng ferritin/mg cell protein. *A. bisporus* degraded 88.69 ± 0.12 % Malachite Green while *G. lucidum* degraded 90.51 ± 0.19 %, maintaining efficiency in both sunlight and UV light. The research indicates that these matrices may serve as valuable nutritional sources and potential substitutes for additives.

1. Introduction

Macro-fungi, commonly known as mushrooms have been widely utilized for their nutritional and medicinal benefits for centuries. These mushrooms are considered an excellent source of protein (Lectins, laccase, and Ergothioneine-binding protein), vitamins (B complex and vitamin D), minerals (such as iron, zinc, calcium, selenium, copper, and potassium), and a variety of other bioactive components (beta-glucan) (Demirtas et al., 2024; Lai et al., 2024; Teli et al., 2024; Yusran et al., 2023). Among all macro-fungi, *Agaricus bisporus*, commonly known as the button mushroom, and *Ganoderma lucidum*, referred to as the reishi or lingzhi mushroom are well known due to their abundance of bioactive compounds and distinct culinary and medicinal reputations (Wickramasinghe et al., 2023). Both species have long been integral components of traditional medicinal systems, with recent scientific investigations exploring their potential roles in functional product development and diverse applications (Wang et al., 2024). However, fresh macro-fungi fruiting bodies are highly perishable, lasting only a few hours at room temperature, therefore to extend their shelf life and broaden their applications these fruiting bodies are often dried and powdered making them easier to store and transport (Pratti et al., 2024). This powdered form retains the nutritional benefits of fresh macro-fungi and is ideal for use in dietary supplements, functional foods, and environmental applications (Demirtas et al., 2024; Shams et al., 2022).

In recent years mushroom powders have also been utilized for their multifaceted industrial applications due to their unique composition and properties (Devi et al., 2024). At the industry level, the techno-functional properties refer to the physical and chemical attributes of

* Corresponding author.
E-mail address: princefoodtech@gmail.com (P. Chawla).

https://doi.org/10.1016/j.fochx.2024.101937
Received 16 September 2024; Received in revised form 21 October 2024; Accepted 25 October 2024
Available online 29 October 2024

the food-based products that impact product formulation like texture, and processing efficiency (Atik et al., 2024; Vélez-Uribe et al., 2023). Mushroom-derived powders, due to their excellent protein and polysaccharide content, exhibit several functionalities including water retention, emulsification, thickening, and fat-binding capacities (Mazumder et al., 2023). As an active food ingredient, its incorporation into food products including bakery items, meat analogs, and soups can improve moisture retention, enhance protein content, and provide antioxidant benefits, overall sensory attributes, and shelf life of the product (Mazumder et al., 2024). Therefore, the growing interest in sustainable natural-based ingredients further highlights the importance of mushroom powder in food applications (Devi et al., 2024). Consequently, it is esteemed not just for its nutritional advantages but also for its capacity to enhance texture, flavor, and usefulness across many food systems, rendering it a versatile and environmentally sustainable option for food innovation (J. Tang et al., 2024).

Mushroom powders, characterized by a variety of polar, non-polar, and surface-active constituents, have garnered interest for their potential applications in environmental bioremediation, especially in the degradation of photocatalytic dyes (Shahid-Ul-Islam et al., 2023). Industrial effluents filled with synthetic dyes pose a significant environmental challenge due to their toxicity, persistence, and impact on aquatic ecosystems (Pandey et al., 2024). To address these issues, researchers have been exploring eco-friendly sustainable methods for dye degradation by involving the use of natural and biologically derived materials as photocatalysts (Khan et al., 2023). Herein, the inherent structure of mushroom powder due to its ability to act as a support or catalyst in the degradation process combined with its ease of functionalization and ability to generate reactive oxygen species under light irradiation, makes it a viable candidate for degrading harmful dyes such as Malachite green and Eosin Y (Liang et al., 2024). Furthermore, mushroom powders are biodegradable, non-toxic, and can be produced at low cost, enhancing their appeal as an environmentally sustainable material for water treatment technologies (Ghose et al., 2024). The integration of mushroom powders into photocatalytic systems offers an innovative method for utilizing natural resources in environmental remediation, thereby advancing the creation of sustainable and effective strategies for industrial wastewater treatment (Sethi et al., 2024).

In addition, mushroom powder has also gained prominence for its high nutritional content, particularly its rich mineral composition (Munir et al., 2023). Minerals like calcium, magnesium, iron, and zinc are essential for various physiological functions in the human body but their bioavailability how effectively they are absorbed and utilized by the body is a critical factor influencing their nutritional benefits (Ghafoor et al., 2024; Iqbal et al., 2024). Inorganic mineral salts present in mushroom powder, while contributing essential nutrients like magnesium and zinc can also lead to toxicity due to the bioaccumulation of heavy metals including cadmium, arsenic, and lead (Ghuniem et al., 2024). The risk of toxicity is sensitive to the ability of mushrooms to absorb these elements from contaminated environments, demanding careful monitoring of mineral concentrations to ensure safe consumption (de Souza et al., 2023). A promising approach for investigating mineral bioavailability involves the utilization of Caco-2 cells, a recognized in vitro model for simulating human intestinal absorption. The Caco-2 cell model, originating from human colon carcinoma cells, replicates the characteristics of intestinal epithelial cells and serves as a dependable instrument for evaluating nutrient transport and absorption across the intestinal barrier (De et al., 2024). Its unique composition of polysaccharides, fibers, and proteins has the potential to enhance mineral solubility and absorption, making it a valuable source for improving mineral intake in diets (Devi et al., 2024). Understanding the bioavailability of minerals from mushroom powder through caco-2 cells provides insights into its nutritional efficacy and highlights its potential role in addressing mineral deficiencies in populations (Quero et al., 2024). This research is crucial for promoting the use of mushroom powder as a functional food ingredient with enhanced health benefits.

The objective of this study is to explore the multifaceted potential of *Agaricus bisporus* and *Ganoderma lucidum* powders by analyzing their proximate composition, techno-functional properties, structural and chemical characteristics, and photocatalytic dye degradation capabilities. Despite recognition of the dietary and environmental applications of these macro-fungi, there exists a notable deficiency in thorough investigations assessing their efficacy in degrading synthetic dyes and their specific structural characteristics. While the nutritional and environmental applications of *Agaricus bisporus* and *Ganoderma lucidum* are acknowledged, little is known about their photocatalytic efficiency in degrading synthetic dyes like Eosin Y and Malachite Green, a potential eco-friendly solution for wastewater treatment. Additionally, the study emphasizes the structural and chemical properties of these fungi, as well as their techno-functional attributes, providing valuable insights into their roles in food and environmental applications. Moreover, the investigation of mineral uptake via Caco-2 cells fills a critical knowledge gap regarding their nutritional bioavailability, making these fungi promising candidates for addressing nutritional deficiencies. By adopting a holistic approach that combines nutritional, structural, and environmental evaluations, the study uniquely contributes to understanding the multifunctional roles of these macro-fungi, offering innovative solutions across industries. The novelty of this research comes under a complete approach by combining a comparative analysis of the techno-functional properties and mineral uptake of *Agaricus bisporus* and *Ganoderma lucidum* with their photocatalytic efficiency in degrading dyes like Eosin Y and Malachite Green. This study presents a detailed analysis of the chemical and structural properties of these macro-fungi, revealing their dual potential for nutritional applications and environmental remediation.

2. Materials and methods

2.1. Biological materials

The fruiting bodies of *Agaricus bisporus* were obtained from the Directorate of Mushroom Research Centre (DMRC), Solan, Himachal Pradesh, India, in March 2024. Whereas, the fruiting bodies of the *Ganoderma lucidum* were collected from the bark of wildly grown Acacia trees available in the farm area of Lovely Professional University, Punjab, India, during August 2023. The Department of Botany, Lovely Professional University, Phagwara, Punjab, India, with the catalog reference LPU22/A789 confirmed the *Ganoderma lucidum* specimens. Chemicals such as petroleum ether, ethanol, sulfuric acid, sodium hydroxide, nitric acid, hydrochloric acid, potassium sulfate, cupric sulfate, and boric acid were procured from Hi Media Chem Pvt. Ltd., Vadodara, Gujarat, India. Eosin Y and Malachite green dye were purchased from Loba Chemie Pvt. Ltd. (Mumbai, India). All the glassware was washed with nitric acid and double distilled water to maintain high standards of precision and purity throughout the experiments.

2.1.1. Sample preparation

Initially, the *Agaricus bisporus* samples were selected based on their freshness indicators, which included white appearance, maturity state, and medium size. Whereas the *Ganoderma lucidum* samples were selected based on their woody appearance, shiny surface, and maturity characteristics. Both samples were carefully washed with distilled water to remove any surface impurities and contaminants. Following this, the fruiting bodies were dried using a tray dryer (Labfit India Pvt. Ltd., Mumbai, India) at 50 °C for 24 h. Post-drying, these fruiting bodies were ground into a fine powder using a mechanical milling device (Rex 900, Bajaj Electricals Ltd., India). The powders were then sieved through a 60-mesh mechanical sieve shaker (Labfit India Pvt. Ltd., Mumbai, India), and the resulting powders were stored in sterilized air-tight glass containers for further analysis.

2.2. Methods

2.2.1. Nutritional characterization

The proximate compositions of both the macro-fungi powders were analyzed following AOAC (2016) protocols. Moisture content was determined by oven drying at 105 °C to a constant weight, then calculating dry matter yield. Crude protein was measured using the Kjeldahl method (KJL-12 L, Pelican Equipment, Chennai) with a 4.38 nitrogen-to-protein conversion factor. Crude fat was estimated via the Soxhlet method using petroleum ether (40–60 °C) as a solvent. The residue post-fat extraction was treated with 1.25 % sulfuric acid and 1.25 % sodium hydroxide to determine crude fiber. Crude ash content was obtained by incinerating samples at 550 °C for 3 h in a muffle furnace. Then the total carbohydrates were estimated using the difference method, as Eq. (1) outlined.

$$\text{Total carbohydrate (\%)} = 100 - (\text{Moisture content} + \text{protein} + \text{fat} + \text{ash content}) \quad (1)$$

2.2.2. Mineral estimation

The mineral content of both the macro-fungi powders was analyzed using Inductively Coupled Plasma Optical Emission Spectroscopy (ICP-OES; Thermo Scientific, iCAP 7000 series, Germany), as detailed in Patil et al. (2024). Laboratory glassware was prepared by soaking in 10 % nitric acid for 24 h, followed by rinsing with deionized water and air drying. The ICP-OES spectrometer was calibrated using the Intelligent Calibration and Logic (ICAL) method from Spectro Analytical Instruments GmbH (2012). A nine-point calibration curve was generated from serial dilutions of a multielement standard solution. Mineral concentrations were determined at specific emission lines: iron (238.204 nm), zinc (213.856 nm), calcium (396.847 nm), copper (324.754 nm), magnesium (285.213 nm), sodium (589.592 nm), and potassium (769.896 nm) using radial plasma observation. No flux or hydrochloric acid was added during calibration to match the sample matrix preparation. Concentrations above 10 mg/L led to precipitate formation due to chloride anions. The accuracy of measurements was verified using an Initial Calibration Verification (ICV) control sample of 20 mg/L for iron, zinc, and calcium, with an acceptance criterion of ±10 %. Control samples were analyzed every ten samples to ensure measurement reliability, following guidelines from Spectro Analytical Instruments GmbH and the U.S. Environmental Protection Agency (EPA).

2.2.3. Characterizations of macro-fungi powder

Both the macro-fungi powders were characterized using various techniques. Field emission scanning electron microscopy (FE-SEM, JEOL-JSM-7610F) was employed to examine surface properties and morphology, following Mat Zin et al. (2022). Samples were mounted on carbon-coated copper tape, gold-coated via sputtering for 3 min at 30 mA, and imaged at 20.0 kV with a focal distance of 7.9–8.0 mm. Fourier transform infrared spectroscopy (FTIR, Perkin Elmer Spectrum Two) was used to identify functional groups in the mid-infrared range of 4000–400 cm^{-1}, with spectra processed using Spectrum 10 software, as described by Akcay et al. (2023). X-ray diffraction (XRD, Bruker) was utilized to obtain spectra within a 2θ range of 10–55° at a 5°/min scanning rate, following Shams et al. (2022). Differential scanning calorimetry (DSC, Perkin Elmer) analyzed thermal properties by heating samples from 30 °C to 450 °C at 10 °C/min under a nitrogen atmosphere, in line with (Zhang et al., 2022). Thermogravimetric analysis (TGA 4000/Pyris 6) assessed thermal degradation from 10 °C to 900 °C at a 10 °C/min scanning rate in a nitrogen environment, following Tsai et al. (2018).

2.2.4. Techno-functional properties

2.2.4.1. Bulk density. The bulk density was measured using a 10 mL measuring cylinder Gong et al., 2022a; Gong et al., 2022b; Gong et al., 2022c). The cylinder was weighed, filled with the powdered macro-fungi sample, and lightly tapped until the volume remained constant, after which the calculation was performed using Eq. (2)

$$\text{Bulk density}\left(\frac{g}{cm^3}\right) = \left[\frac{\text{Weight of powder sample}}{\text{Volume of sample after tapping}}\right] \quad (2)$$

2.2.4.2. Water and oil holding capacity. Water and oil absorption capacities were evaluated according to the methodology outlined by (Yılmaz & Zungur Bastıoğlu, 2020). A 50 mL centrifuge tube was weighed, and 1 *g* of powdered sample was added, followed by 10 mL of distilled water in one set and soybean oil in another. These mixtures were left to stand for 30 min. The tubes were then centrifuged at 27 °C for 5 min at 5000 rpm. After centrifugation, the supernatant was removed, and the tubes with the sedimented pellets were reweighed. The absorption capacity was calculated as grams of water or oil absorbed per gram of sample. The capacity of the samples to bind water or oil was quantified as grams of water or oil absorbed per gram of the sample, calculated using Eq. (3).

$$\text{Water and oil holding capacity (g/g)} = \left[\frac{\text{weight of centrifuge with a dry mass (g)} - \text{the weight of the centrifuge with a wet mass (g)}}{\text{Initial weight of the sample}}\right] \times 100 \quad (3)$$

2.2.4.3. Emulsifying capacity. The emulsifying capacity and stability of the macro-fungi powders were assessed using the method by (Fan et al., 2021). Briefly, 2 g of powdered sample was mixed with 200 mL of water to form a 1 % (*w/v*) solution, then 2 mL of soybean oil (2 % *v/v*) was added. The mixture was stirred at 2000 rpm for 1.5 h with a magnetic stirrer to create a milky emulsion. The emulsion was then centrifuged at 10,000 ×*g* for 20 min. The volume of the emulsified layer was accurately measured using a calibrated measuring cylinder, and the emulsification efficiency was determined using a specific Eq. (4).

$$\text{Emulsifying capacity (\%)} = \left[\frac{\text{Emulsified volume (ml)}}{\text{Total volume (ml)}} \times 100\right] \quad (4)$$

To assess emulsion stability, samples were heated to 90 °C in a water bath for 20 min, then centrifuged at 10,000 ×*g* for 20 min. The formation of a two-phase suspension indicated emulsification capacity and stability was determined using Eq. (5).

$$\text{Emulsifying stability (\%)} = \left[\frac{\text{Height of emulsified layer after heating (cm)}}{\text{Emulsified layer before heating (cm)}} \times 100\right] \quad (5)$$

2.2.4.4. Foaming capacity and stability. The foaming ability and stability of the powdered samples were evaluated using the method (Sharma et al., 2023). A 2 % (*w/v*) solution was made by dissolving 5 g of the sample in 200 mL of distilled water, then stirring vigorously for 5 min with a high-speed mixer. The mixture was poured into a graduated cylinder to measure the initial and final volumes before and after foaming. The foaming capacity was then determined by calculating the percentage volume increase using a specific Eq. (6).

$$\text{Foaming capacity (\%)} = \left[\frac{\text{Volume of foam after whipping (mL)} - \text{the volumefoam before whipping (mL)}}{\text{The volume foam before whipping (mL)}} \times 100\right] \quad (6)$$

Foaming stability was determined by the change in initial foam volume at 28 °C for 30 min and 1 h and calculated using Eq. (7).

$$\text{Foaming stability (\%)} = \left[\frac{\text{Volume after resting (30 } min\text{)} - \text{volume before resting}}{\text{Volume before resting}} \times 100\right] \quad (7)$$

2.2.5. Mineral bioavailability

2.2.5.1. In vitro mineral bioavailability. To evaluate the in vitro bioavailability of iron, zinc, and calcium in both the macro-fungi powders, the following methodology (Kała et al., 2021) was employed. The study aimed to measure the absorption and utilization efficiency of these minerals by the human body. The experiment simulated gastrointestinal digestion and used Caco-2 cell lines in a trans-well assay to assess cellular absorption. The aim was to understand the bioavailability of minerals from macro-fungi powders and highlight their potential nutritional benefits for human health.

2.2.5.2. Simulated gastrointestinal digestion. A simulated gastrointestinal digestion was performed according to the procedure to evaluate the bioavailability of iron, zinc, and calcium in both the macro-fungi powders (Hu et al., 2023). The process began with mixing 5 mL of the sample with 1.90 mL of saliva solution in a conical flask, followed by incubation at 35 °C and 95 rpm for 10 min. Next, 3.1 mL of gastric juice was added, and the pH was adjusted to 2 using hydrochloric acid (HCl). The mixture was then incubated at 35 °C in the dark for 2 h to simulate gastric digestion. Subsequently, 1.97 mL of bile juice and 5.30 mL of duodenal juice were added to simulate intestinal digestion, with a 3 h incubation. After digestion, the mixture was centrifuged using a 10 KDa ultrafiltration centrifuge tube to isolate the soluble fraction. The bioavailability of iron, zinc, and calcium was determined based on their concentrations in the soluble fraction, representing the proportion of each mineral available for absorption from the macro-fungi powder.

$$\text{Mineral bioavailability (\%)} = \left[\frac{\text{concentration of dialysate (Permeate)}}{\text{concentration of the sample}} \times 100\right] \quad (8)$$

2.2.5.3. Cellular absorption study (trans-well assay). Caco-2 cells were cultured using the methodology (Lavanya et al., 2023). The growth medium included 39 μg/mL Streptomycin, 25 μg/mL Amphotericin, 100 μg/mL Penicillin, 2 mM L-Glutamine, 10 % heat-inactivated fetal bovine serum, and 1 % DMEM. Cells were incubated at 35 °C with 96 % humidity and 4 % CO_2 and the medium was replaced every other day. The cells were passaged at approximately 90 % confluence, typically within 7–8 days, using 0.05 % EDTA and 0.5 % trypsin. At the 39th passage, cells were seeded at 50,000 cells per well in six-well plates with sterile polyester membranes (24 mm diameter, 0.4 μm pore size) for mineral absorption assays. Differentiation occurred in a CO_2 incubator, with the medium refreshed every other day and cells washed five times with PBS. After an initial 4–5 days, cells underwent a 10-day differentiation period before the transepithelial cellular absorption assay was conducted.

2.2.5.4. Valuation of cell monolayer integrity. Regular assessments of the morphological properties and impurity detection in Caco-2 cells were conducted using inverted light microscopy (Saxami et al., 2021). Once the cells achieved full coverage, their quality was further evaluated with a phenol red dye test. Following cell washing, 2 mL of PBS (phosphate-buffered saline) was added to the lower compartment, and 2 mL of DMEM containing phenol red dye was added to the upper compartment. After an incubation period, a 100 μL sample was collected from both compartments. The amount of phenol red that permeated into the lower compartment was quantified using an automated ELISA plate reader (Beckman Coulter, Brea, USA) at a wavelength of 558 nm.

2.2.5.5. Transport studies of mineral. Pre-washed cells were exposed to 2 mL of DMEM containing 50 μM mineral dialysate from simulated gastrointestinal digestion to study the transepithelial transport of minerals (Nambafu et al., 2023). This medium was added to the upper surface of the cells, while 2 mL of DMEM was added to the lower compartment. After a 3 h incubation at 37 °C, the DMEM was removed to evaluate mineral absorption across the cell line. The cells were then cultured for an additional 22 h to induce ferritin synthesis. Mineral transfer across the cellular barrier from both compartments was analyzed using the ICP-OES method.

2.2.5.6. Ferritin content. To evaluate the cellular ferritin accumulation, pre-washed cells were detached using trypsin further collected, and re-suspended in 2 mL of cell-grade water. The cells were then lysed using a probe sonicator at 4 °C for 2 min, with 5 s pulses to release intracellular ferritin. The ferritin content was quantified using a Human Ferritin ELISA kit (Thermo Fisher Scientific). In this assay, the cell lysates were added to ELISA plate wells previously coated with ferritin-specific antibodies. After incubation, unbound materials were washed away, and a detection antibody conjugated with an enzyme was added to bind ferritin. A substrate (Tetramethylbenzidine) was introduced to generate a color change, which was proportional to the ferritin concentration. The reaction was stopped, and absorbance was recorded at 450 nm, allowing ferritin levels to be quantified using a standard curve based on known ferritin concentrations.

2.2.6. Photocatalytic dye degradation potential of macro-fungi species

The dye reduction effectiveness of powdered macro-fungi samples through photocatalysis was tested following a modified version of the procedure by (Manimaran et al., 2023). Two dyes, Eosin Y (anionic) and Malachite Green (cationic), each at 10 ppm concentration, were used. The degradation capacity was assessed under direct sunlight and UV light (Philips, 150 W, 200–280 nm) in the presence of the macro-fungi powder. The dye and macro-fungi powder mixture was magnetically stirred at 150 rpm in the dark for 30 min to establish absorption and

Table 1
Proximate compositions of *Ab* (*Agaricus bisporus*) and *Gl* (*Ganoderma lucidum*).

	Agaricus bisporus	*Ganoderma lucidum*
Moisture (%)	69.49 ± 0.62^{b}	58.87 ± 0.28^{a}
Ash (%)	6.68 ± 0.22^{b}	4.43 ± 0.47^{a}
Fat (%)	1.58 ± 0.43^{b}	1.56 ± 0.29^{a}
Fiber (%)	5.66 ± 0.42^{a}	15.53 ± 0.35^{b}
Protein (%)	12.51 ± 0.21^{b}	11.08 ± 0.84^{a}
Carbohydrate	3.57 ± 0.35^{a}	4.52 ± 0.26^{b}

Results are expressed as mean (n = 3) ± standard deviation. The uppercase letters a and b denote differences with in a row and values followed by the same letter in a row do not differ significantly ($p < 0.05$).

desorption equilibrium before light exposure. A solution containing 25 mL of dye and 100 mg of macro-fungi powder was continuously stirred in a conical flask. The solutions were then exposed separately to UV light and sunlight. Aliquots of 2 mL were taken at 10-min intervals, and centrifuged at 10,000 ×*g* for 15 min, and the remaining dye concentration was measured using UV–visible spectroscopy (Shimadzu UV-1800, Japan) to determine degradation efficiency. The dye degradation efficiency (%) was calculated using Eq. (9).

$$\text{Dye degradation efficiency } (\%) = [C_o/C_t \times 100\,] \tag{9}$$

where 'C_0' and 'C_t' were the initial and remaining dye concentrations (mg L^{-1}) of the aqueous solution in a given time, respectively. The kinetics study of the photocatalytic decolorization rate of Eosin Y and Malachite green was determined using the Langmuir Hinshelwood kinetics model as given in Eq. (10).

$$ln\frac{C_o}{C_t} = kt \tag{10}$$

2.3. Statistical analysis

All experiments were conducted with a minimum of three independent determinations, and the results are reported as mean ± standard deviation. Statistical analysis was performed using one-way ANOVA and Duncan's multiple-range tests to identify significant differences. Mean comparisons were made using the critical difference (CD value), utilizing the data analysis tool pack in Microsoft Excel® 2019 (Microsoft Corp., Redmond, USA). Average values and standard deviations were also calculated using this software.

3. Results and discussions

3.1. Proximate analysis

The proximate compositions of *A. bisporus* and *G. lucidum* powder are presented in Table.1. The higher moisture content in *A. bisporus* (69.49 ± 0.62 %) compared to *G. lucidum* (58.87 ± 0.28 %) is influenced by factors such as harvesting time, maturation period, and the specific humidity and temperature conditions during growth, as well as storage conditions (Petre & Teodorescu, 2020a; Petre & Teodorescu, 2020b; Tang et al., 2021). *A. bisporus* is typically grown in a more controlled, moisture-rich environment, whereas *G. lucidum* grows in drier, tougher substrates, resulting in lower moisture content. The shelf life of macro-fungi is greatly influenced by the measurement of the moisture content. However, the higher protein content in *A. bisporus* (12.51 ± 0.21 %) than that of *G. lucidum* (11.08 ± 0.84 %) can be attributed to its cultivation in nutrient-rich substrates, which promote protein synthesis. The significant difference in ash content, with *A. bisporus* having higher levels (6.68 ± 0.22 %) than *G. lucidum* (4.43 ± 0.47 %), reflects the mineral content of their respective growing mediums and the metabolic processes specific to each species. Both macro-fungi exhibit low-fat content, which is typical of macro-fungi, but the fiber content is significantly higher in *G. lucidum* (15.53 ± 0.35 %) compared to *A. bisporus* (5.66 ± 0.42 %) due to the tougher, more fibrous structure of *G. lucidum*, which aids in its survival in harsh environments. Moreover, the higher carbohydrate content in *G. lucidum* (4.52 ± 0.26 %) than in *A. bisporus* (3.57 ± 0.35 %) could be related to its need for energy storage in its challenging growth conditions. These differences illustrate the impact of species-specific traits, environmental conditions, and growth substrates on the nutritional profiles of these macro-fungi (Kalač, 2016a; Kalač, 2016b). This aligns with Breene's (1990) research, which found that macro-fungi typically comprise about 90 % water, with proteins ranging from 10 % to 40 %, fats between 2 % and 8 %, carbohydrates making up 3 % to 28 %, fiber from 3 % to 32 %, and ash constituting 8 % to 10 %. However, variations in climate, species, and geographical regions can influence these values.

Table 2
Mineral content of *Agaricus bisporus* and *Ganoderma lucidum*.

Minerals	*Agaricus bisporus* (ppm)	*Ganoderma lucidum* (ppm)
Iron	5.9384 ± 0.34^{a}	24.6341 ± 0.87^{b}
Zinc	6.4317 ± 0.24^{a}	7.9673 ± 0.39^{b}
Calcium	36.2984 ± 0.98^{b}	19.8314 ± 0.81^{a}
Copper	59.9117 ± 0.47^{b}	24.9313 ± 0.62^{a}
Magnesium	89.8255 ± 0.72^{b}	78.7325 ± 0.88^{a}
Sodium	49.9824 ± 0.81^{b}	29.7688 ± 0.79^{a}
Potassium	4159.2387 ± 23.97^{a}	4332.6945 ± 26.94^{b}

Results are expressed as mean (n = 3) ± standard deviation. The uppercase letters a and b denote differences with in a row and values followed by the same letter in a row do not differ significantly ($p < 0.05$).

3.2. Mineral content

Certain mineral components from *A. bisporus* and *G. lucidum* are shown in Table. 2, measured in parts per million with significant differences in their nutritional profiles. The mineral analysis of *G. lucidum* revealed significantly higher levels of iron 24.6341 ± 0.87 ppm, zinc 7.9673 ± 0.39 ppm, and potassium 4332.6945 ± 26.94 ppm, making it a superior source for these minerals, which are essential for immune function, cardiovascular health, and muscle contraction. In contrast, *A. bisporus* exhibits significantly higher concentrations of calcium 36.2984 ± 0.98 ppm, copper 59.9117 ± 0.47 ppm, magnesium 89.8255 ± 0.72 ppm, and sodium 49.9824 ± 0.81 ppm. The significant differences in mineral content in both the macro-fungi can be attributed to genetic variability, growth environment, physiological differences, nutritional strategies, and evolutionary adaptations. Each species holds distinct metabolic pathways influenced by their genetic makeup, affecting how they uptake, accumulate, and store minerals. The substrates on which these fungi grow, such as wood for *G. lucidum* and compost for *A. bisporus*, significantly impact their mineral content (Valverde et al., 2015a; Valverde et al., 2015b). Additionally, the mycelial structure, growth rate, and specific saprotrophic behaviors of each species contribute to these differences. The evolutionary pressures have resulted in selective uptake mechanisms that enable each fungus to flourish within its ecological niche and accumulate minerals advantageous for its survival and medicinal attributes. Consequently, *G. lucidum* exhibits higher levels of iron, zinc, and potassium, while *A. bisporus* showed greater concentrations of calcium, copper, magnesium, and sodium highlighting the health benefits. (Haro et al., 2020a; Haro et al., 2020b; Haro et al., 2020c) determined Ca, Mg, K, Na, Fe, Cu, and Zn from 18 species of wild-growing mushrooms and suggested a high content of Fe in various mushroom species.

3.3. Structural characterization

3.3.1. Field emission scanning Electron microscope

The morphology and microstructure of the *A. bisporus* and *G. lucidum* powder were examined using scanning electron microscopy and results are presented in Fig. 1A. The micrographs of *A. bisporus* exhibit a

smoother surface with densely packed microstructures and the presence of individual spherical particles with different sizes in diameter distributed evenly without clustering together at 1000 × magnification (Du et al., 2018a; Du et al., 2018b). However, the micrographs of *G. lucidum* exposed a rougher texture with distinct features like pores or ridges reflecting its role in nutrient absorption. Focusing on its spores and mycelial structures showing a predominantly fibrous morphology characterized by extensive interlinking at 1000 × magnification (Huang et al., 2019a; Huang et al., 2019b). Especially, the mycelium contained septa and showed early signs of spore germination. The spores themselves displayed textured surfaces at their points of germination; these observations showed that *G. lucidum* grows radially without the formation of upward-reaching hyphae. The processing methods such as grinding further influence the differences with *A. bisporus* undergoing more uniform grinding while the fibrous nature of *G. lucidum* leads to more fragmented and uneven particles. Ozel and Elibol (2024) determined the surface morphology of chitin chitosan, a major component of macro-fungi.

3.3.2. *Differential scanning calorimetry*

The differential scanning calorimetry thermogram of the *A. bisporus* and *G. lucidum* powder revealed the endothermic transition that may be due to the water loss and thermal degradation of polysaccharides Fig. 1B. The thermogram of *A. bisporus* powder exhibits higher onset

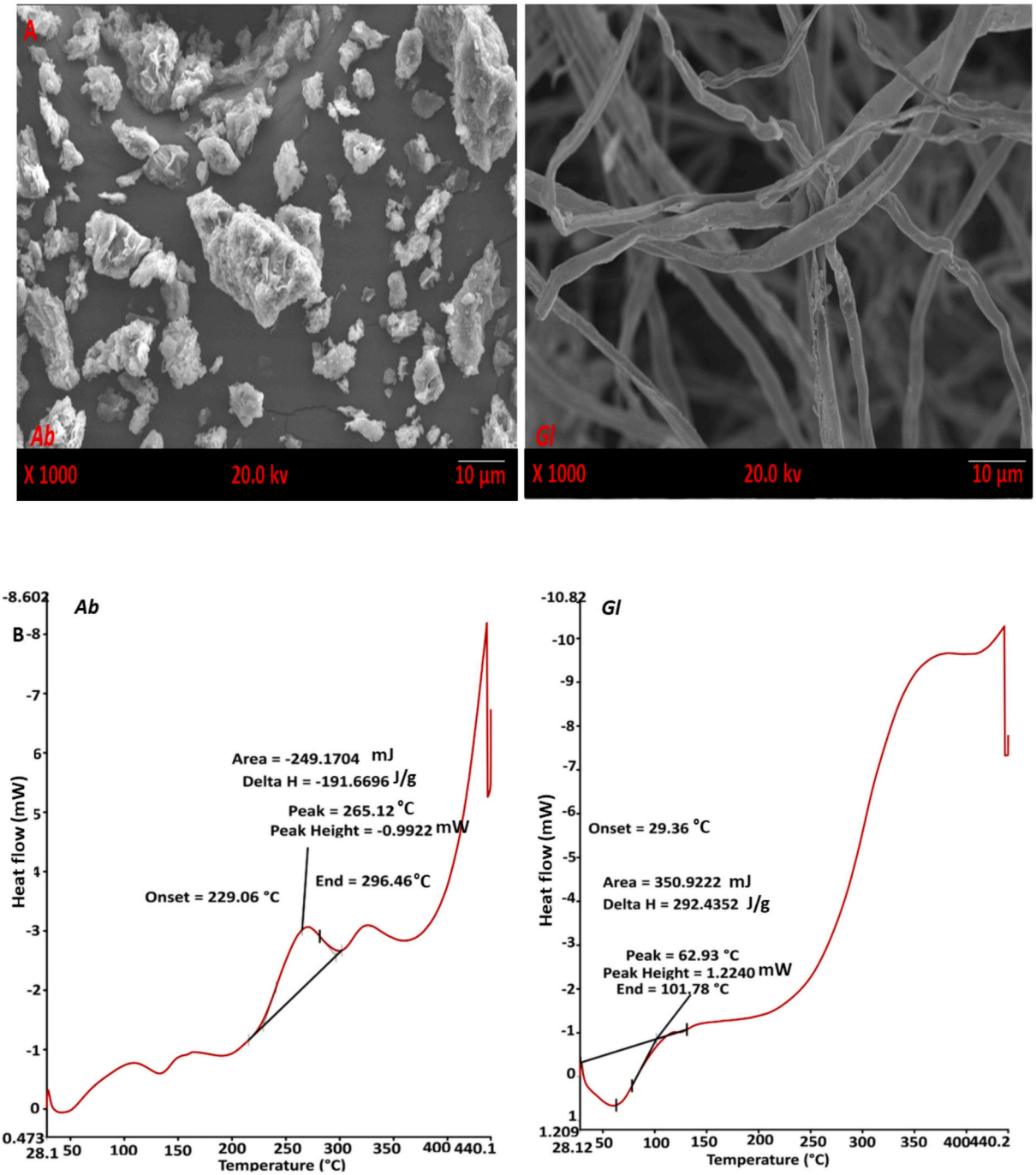

Fig. 1. A. Scanning electron microscopy (SEM) of *Ab* (*Agaricus bisporus)* and *Gl* (*Ganoderma lucidum*), B. Differential scanning calorimetry (DSC) thermograms of *Ab* (*Agaricus bisporus*) and *Gl* (*Ganoderma lucidum*), C. Thermogravimetric analysis (TGA) of *Ab* (*Agaricus bisporus*) and *Gl* (*Ganoderma lucidum*), D. Fourier transform infrared spectroscopy of *Ab* (*Agaricus bisporus*) and *Gl* (*Ganoderma lucidum*), E. X-ray diffraction (XRD) of *Ab* (*Agaricus bisporus*) and *Gl* (*Ganoderma lucidum*)

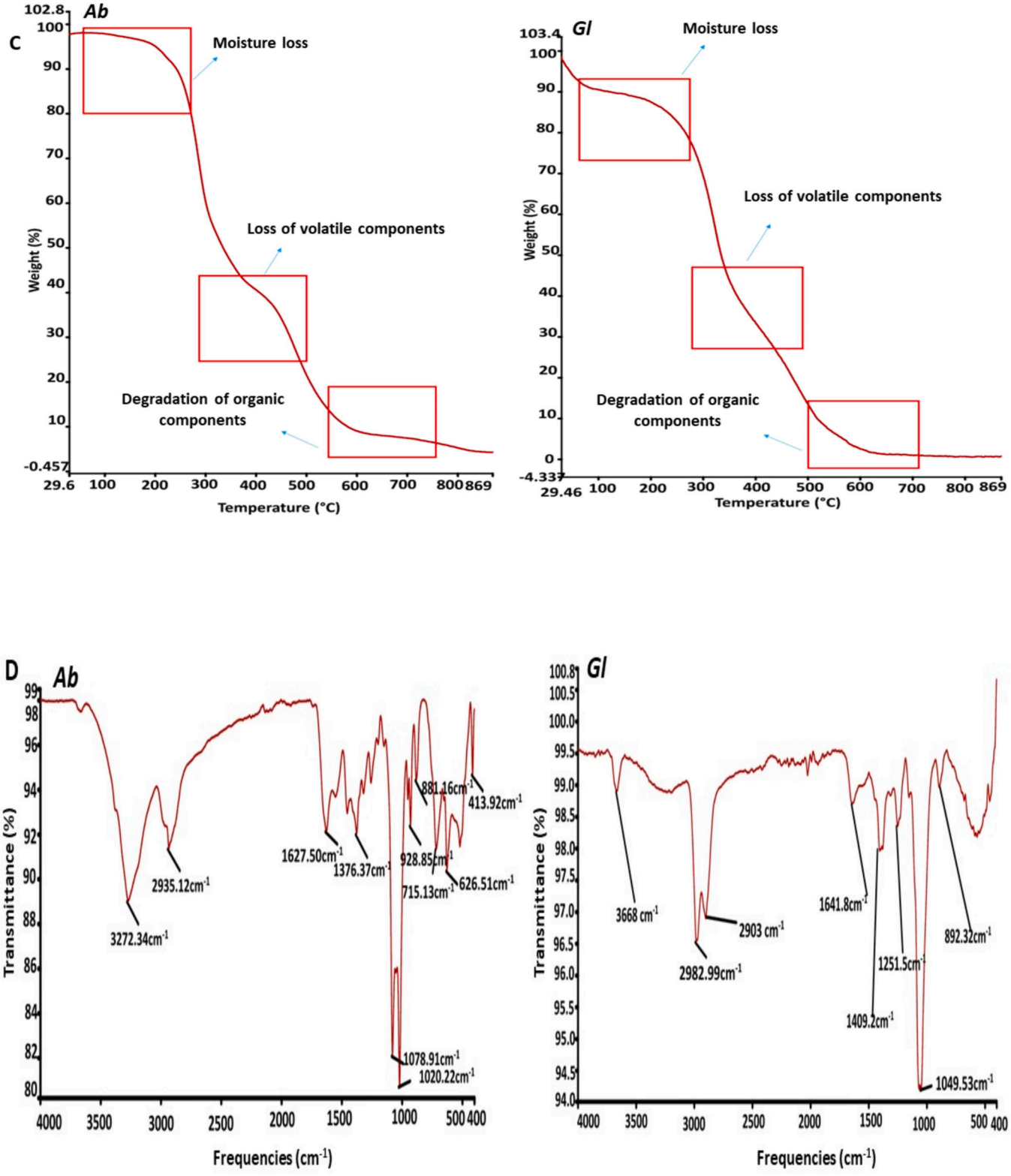

Fig. 1. (*continued*).

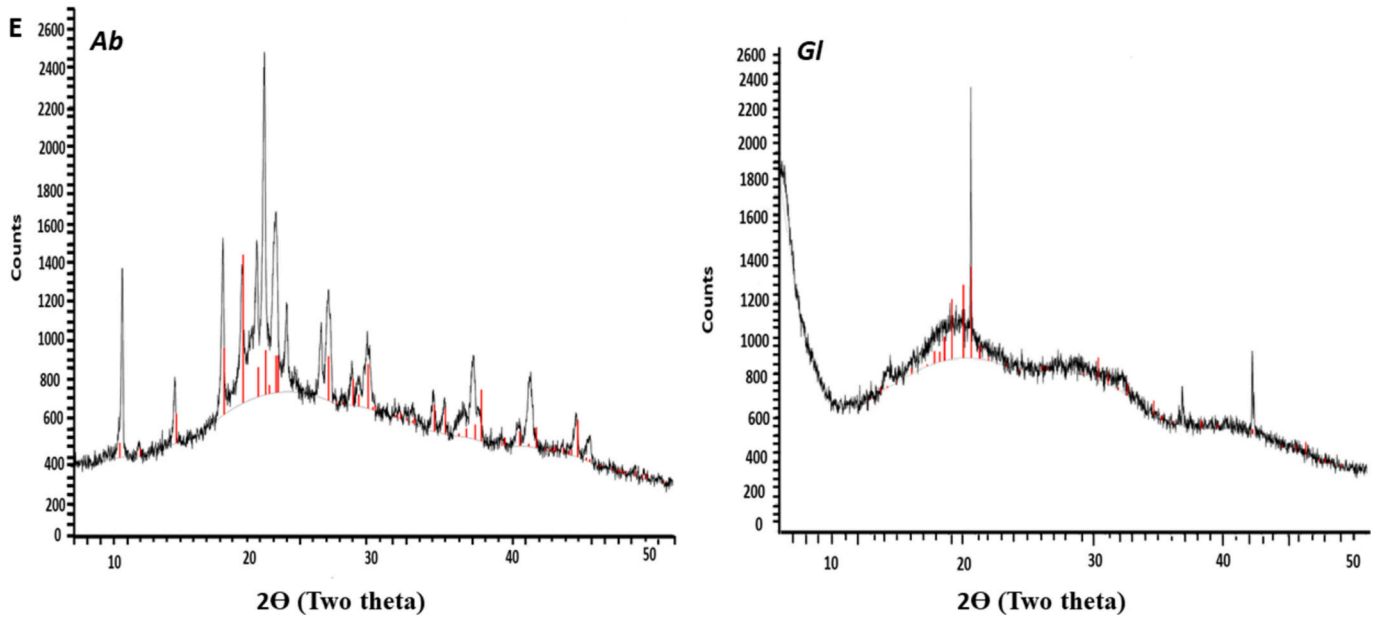

Fig. 1. (*continued*).

(229.06 °C), peak (265.12 °C), and end temperatures (296.46 °C) with a total heat absorption of −191.6696 J/g indicating greater thermal stability. This stability suggests that *A. bisporus* consists of more thermally stable components such as proteins and polysaccharides that require higher temperatures to decompose. The compact and dense microstructure of *A. bisporus* further contributes to its higher thermal resistance (Zheng et al., 2020a; Zheng et al., 2020b). In contrast, the thermogram of *G. lucidum* powder shows lower onset (29.36 °C), peak (62.93 °C), and end temperatures (101.78 °C) with a much higher heat absorption (292.4352 J/g). The lower onset temperature indicates that *G. lucidum* begins to decompose at much lower temperatures reflecting the presence of more thermally labile compounds. The higher heat absorption suggests that *G. lucidum* possesses complex molecular structures such as higher fiber content and intricate polysaccharides which require more energy to break down during thermal decomposition (Liu et al., 2018a; Liu et al., 2018b). These complex molecules decompose over a broader temperature range leading to the higher overall energy absorption. Shams et al. (2022) noted that incorporating *A. bisporus* powder improved the physiochemical and functional properties of cookies.

3.3.3. Thermogravimetric analysis

The thermal stability of *A. bisporus* and *G. lucidum* powder was evaluated utilizing thermogravimetric analysis and the results are represented in Fig. 1C. For *A. bisporus*, the TGA curve shows a significant weight loss of 93.45 % indicating extensive decomposition. This substantial thermal decomposition is primarily due to the loss of moisture, and volatiles, and the breakdown of organic components such as carbohydrates, proteins, and lipids. The peaks in the derivative weight % curve correspond to specific temperatures at which these components decompose highlighting the multi-stage nature of its thermal degradation process (Ying et al., 2019a; Ying et al., 2019b). In contrast, *G. lucidum* exhibits slightly higher thermal stability with a total weight loss of 97.825 %. The higher total weight loss percentage suggests that while a larger portion of the sample decomposes it does so more gradually and over a broader temperature range reflecting better thermal stability (Guo et al., 2021a; Guo et al., 2021b). This higher stability can be attributed to the compositional differences between the two species. *G. lucidum* likely contains a higher proportion of thermally resistant compounds such as complex polysaccharides, lignin-like substances, and chitin which are known to degrade at higher temperatures and more slowly compared to the simpler organic compounds found in *A. bisporus*. Similar findings were observed by (Kim et al., 2021a; Kim et al., 2021b; Kim et al., 2021c) characterization of chitin-glucan complexes derived from mushrooms.

3.3.4. Fourier transform infrared spectroscopy (FT-IR)

Functional groups of molecular components of *Agaricus bisporus* and *Ganoderma lucidum* powder were determined using FTIR analysis and the FTIR spectra represented in Fig. 1D. The spectra of *G. lucidum*, the peak at 3668.00 cm^{-1} and in *A. bisporus* at 3272.34 cm^{-1} indicate hydroxyl groups suggesting higher alcohol or phenolic content in *G. lucidum*. Peaks around 2903.00 cm^{-1} for *G. lucidum* and 2935.12 cm^{-1} for *A. bisporus* indicate CH stretching vibrations typical of -CH2- or -CH3 groups. The amide I band linked to proteins or peptides appears at 1641.80 cm^{-1} for *G. lucidum* and 1627.50 cm^{-1} for *A. bisporus*. The fingerprint region below 1500.00 cm^{-1} shows unique peaks for each macro-fungi such as 1251.5 cm^{-1} and 892.32 cm^{-1} for *G. lucidum* and 1078.91 cm^{-1} and 1020.22 cm^{-1} for *A. bisporus* highlighting their molecular diversity (Reis et al., 2017a; Reis et al., 2017b). These differences suggest variations in polysaccharides, lipids, and secondary metabolites as supported by Y. Zhang et al. (2024), who found appreciable O—H groups enhancing adsorption performance in macro-fungi.

Table 3
Techno-functional properties of *Ab* (*Agaricus bisporus*) and *Gl* (*Ganoderma lucidum*).

	Agaricus bisporus	*Ganoderma lucidum*
Bulk density (g/cm^3)	0.45 ± 0.25^a	0.52 ± 0.28^b
Water holding capacity (g/g)	2.67 ± 0.24^a	3.03 ± 0.05^b
Oil holding capacity (g/g)	2.58 ± 0.34^a	3.25 ± 0.12^b
Emuslifying activity (%)	61.47 ± 0.35^b	59.52 ± 0.38^a
Emulsifying stability (%)	68.26 ± 0.52^b	65.52 ± 0.34^a
Foaming capacity (%)	62.59 ± 0.35^b	59.50 ± 0.28^a
Foaming stability (%)	58.35 ± 0.27^a	59.56 ± 0.23^b

Results are expressed as mean (n = 3) ± standard deviation. The uppercase letters a and b denote differences with in a row and values followed by the same letter in a row do not differ significantly ($p < 0.05$).

3.3.5. X-ray diffraction (XRD)

The differences in the powder properties of *A. bisporus* and *G. lucidum*, as revealed by X-ray diffraction (XRD) analysis provide a detailed view in Fig. 1E attributed to their distinct biochemical compositions and crystalline structures. Herein, *A. bisporus* showed numerous sharp peaks in the XRD spectrum indicating a highly crystalline structure with well-defined stable components such as sodium iron 4-(2-pyridyl azo) resorcinol dihydrate with a triclinic lattice structure. This crystalline nature is a result of its specific mineral content and the orderly arrangement of its molecular components. The presence of such sharp peaks signifies the presence of a regular, repeating crystalline lattice which is typical for compounds with a high degree of crystallinity and structural stability (Hassan et al., 2020a; Hassan et al., 2020b). Whereas, *G. lucidum* exhibits a different set of peaks including

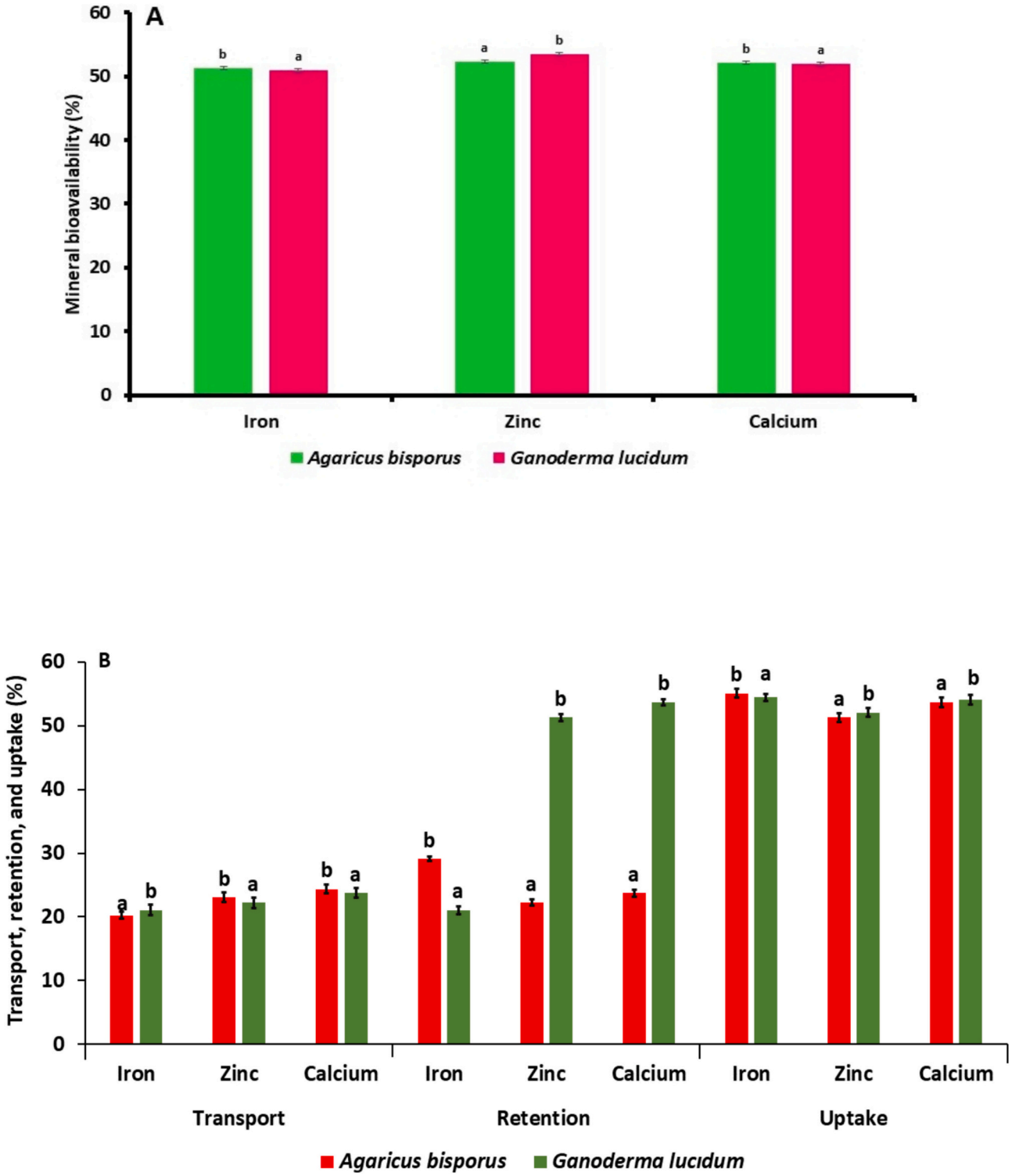

Fig. 2. A. Mineral bioavailability (%), B. Mineral transport, retention, and uptake. The results were expressed as the mean ± standard deviation of ($n = 3$) independent replicates, and error bars represent the standard deviation from the mean values, while different lowercase letters (a and b) above each bar represent significantly different ($p < 0.05$) values based on analysis of variance (ANOVA) and *t*-tests.

both sharp and blunt peaks. This pattern reflects the presence of a variety of bioactive components such as triterpenoids and polysaccharides which contribute to its unique biochemical composition. The sharp peaks indicate regions of high crystallinity, while the blunt peaks suggest amorphous or less-ordered regions within the material (Cao et al., 2021a; Cao et al., 2021b). This combination indicates that *G. lucidum* has a more complex and heterogeneous structure with both crystalline and amorphous phases. The polysaccharides tend to form semi-crystalline or amorphous regions due to their large, complex, and irregular molecular structures. These findings align with Gao, Chang, et al. (2023); Gao, Li, et al. (2023), who studied the structural characteristics of glycoproteins in shiitake mushrooms.

3.4. Functional properties

3.4.1. Bulk density

The bulk density measured in g/cm^3 indicates a substance's compactness as shown in Table 3 in which *A. bisporus* possessed a lower bulk density of 0.45 ± 0.25 g/cm^3 suggesting a lighter, less compact structure (Tian et al., 2019a; Tian et al., 2019b). Whereas, *G. lucidum* exhibits a higher bulk density of 0.52 ± 0.28 g/cm^3 reflecting its tougher, more fibrous nature, and lower water content (Yang et al., 2019a; Yang et al., 2019b). The results are consistent with the research conducted by Zhang et al. (2024), which examined the bulk density of different mushroom species.

3.4.2. Water and oil holding properties

The water-holding capacity (WHC) and oil-holding capacity (OHC) of *A. bisporus* and *G. lucidum* reveal notable differences as shown in Table 3. Herein, *A. bisporus* has a WHC of 2.67 ± 0.24 % and an OHC of 2.58 ± 0.34 % indicating a balanced affinity for water and oil which is an important parameter for texture, flavor, and nutrition. However, *G. lucidum* exhibits significantly higher values with a WHC of 3.03 ± 0.05 % and an OHC of 3.25 ± 0.12 % likely due to its rich polysaccharide content which enhances water retention. The difference in these capacities is influenced by factors such as amino acid composition, protein molecular weight, and surface polarity. Additionally, foods exhibiting high oil binding values preserve desirable texture and inhibit the loss of oil and aromatic compounds. Polysaccharides and proteins in these macro-fungi increase their capacity for water affinity and retention. Likewise, Yılmaz and Zungur Bastıoğlu (2020) noted the drying impact on macro-fungi properties.

3.4.3. Emulsifying capacity and stability

The emulsifying activity and stability of *A. bisporus* and *G. lucidum* have been shown in Table. 3 highlighting their potential as natural emulsifiers. Herein, *A. bisporus* exhibits a significantly higher emulsifying capacity (61.47 ± 0.35 %) compared to *G. lucidum* (59.52 ± 0.38 %) majorly due to its superior protein extracts with better surface-active properties. The difference in these properties helps reduce the interfacial tension between oil and water facilitating stable emulsion formation. Moreover, *A. bisporus* also shows significantly higher emulsion stability (68.26 ± 0.52 %) than that of *G. lucidum* (65.52 ± 0.34 %). This aligns with the findings of Smith et al. (2022) who studied the emulsifying properties of *Ganoderma* species powders.

3.4.4. Foaming capacity and stability

The foaming properties of *A. bisporus* and *G. lucidum* were compared and shown in Table. 3 revealing that *A. bisporus* significantly has a higher foaming capacity (62.59 ± 0.35 %) than *G. lucidum* (58.35 ± 0.27 %). This suggests that *A. bisporus* proteins may better reduce surface tension resulting in stable foam formation. While *G. lucidum* exhibits significantly greater foaming stability (59.56 ± 0.23 %) than *A. bisporus* 58.35 ± 0.27 % due to its unique surface-active compounds creating more elastic films at the air-water interface. These foaming properties are crucial for the texture and quality of food products, as noted by Jin et al. (2022) in their study of *Pleurotus geesteranus* proteins.

3.5. In-vitro mineral bioavailability

The in vitro mineral bioavailability differences between *A. bisporus* and *G. lucidum* powders stem from their distinct mineral compositions, binding components, structural characteristics, and interactions with digestive conditions. *G. lucidum's* higher levels of iron (24.6341 ± 0.87 ppm), zinc (7.9673 ± 0.39 ppm), and potassium (4332.6945 ± 26.94 ppm) which are essential for immune function and cardiovascular health. However, the higher level of calcium in *A. bisporus* (36.2984 ± 0.98 ppm), copper (59.9117 ± 0.47 ppm), magnesium (89.8255 ± 0.72 ppm), and sodium (49.9824 ± 0.81 ppm) supports the bone health and metabolic processes. Moreover, in *G. lucidum* polysaccharides and triterpenoids can enhance or inhibit mineral absorption by forming soluble or insoluble complexes, while protein and amino acids in *A.* bisporus may enhance bioavailability through chelation. The fibrous structure of *G. lucidum* slows digestion but promotes sustained mineral release whereas the compact structure of *A. bisporus* may facilitate quicker digestion and faster mineral release. The interplay of these characteristics, together with the mineral content of each species and its interaction with digestive pH and enzymes, collectively affects the effectiveness of mineral absorption and utilization from these macro-fungi powders. These findings indicate that both macro-fungi offer unique therapeutic benefits, making them valuable dietary additions. Haro et al. (2020a); Haro et al. (2020b); Haro et al. (2020c) also noted high iron content in various wild-growing mushrooms.

3.5.1. Mineral uptake by Caco-2 cells

The mineral uptake by Caco-2 cells between *A. bisporus* and *G. lucidum* powder is shown in Fig. 2. B revealed by the trans-well assay following simulated gastrointestinal digestion which can be attributed to their unique biochemical compositions and specific mineral-binding properties. *G. lucidum* demonstrated significantly higher iron transport (21.05 ± 0.03 %) but lower retention compared to *A. bisporus* despite both exhibiting similar iron uptake (55.09 ± 0.06 %). This suggests that iron content in *G. lucidum* may be more bioavailable initially but less stable for cellular retention due to the presence of polysaccharides and triterpenoids that enhance iron solubility and initial transport but do not facilitate retention. However, *A. bisporus* with higher protein and organic acid content may better stabilize iron within cells improving retention. For zinc, *A. bisporus* exhibited significantly higher transport (23.07 ± 0.09 %) majorly due to its protein content aiding in zinc chelation and transport. Moreover, *G. lucidum* showed significantly greater retention (51.28 ± 0.06 %) and similar uptake (52.06 ± 0.04 %) indicating that its polysaccharides and fibrous structure may create a more controlled release of zinc, facilitating higher cellular retention. Regarding calcium, *G. lucidum* displayed significantly lower transport (23.73 %) but higher retention (53.71 ± 0.03 %) and comparable uptake (54.05 ± 0.11 %). The high retention of calcium in *G. lucidum* could be due to its complex polysaccharides and fibrous components that

Table 4
Ferritin synthesis in Caco-2 cells from *Ab* (*Agaricus bisporus*) and *Gl* (*Ganoderma lucidum*).

	Ferritin synthesis in Caco2 cells	
	ng ferritin. mg cell protein^{-1}	ng ferritin. mg cell protein^{-1}. g sample^{-1}
Media	2.51 ± 0.04	–
Agaricus bisporus	25.17 ± 0.52^a	130.38 ± 0.49^a
Ganoderma lucidum	28.68 ± 0.61^b	141.55 ± 0.56^b

Results are expressed as mean (n = 3) ± standard deviation. The uppercase letters a and b denote differences with in a column and values followed by the same letter in a column do not differ significantly ($p < 0.05$).

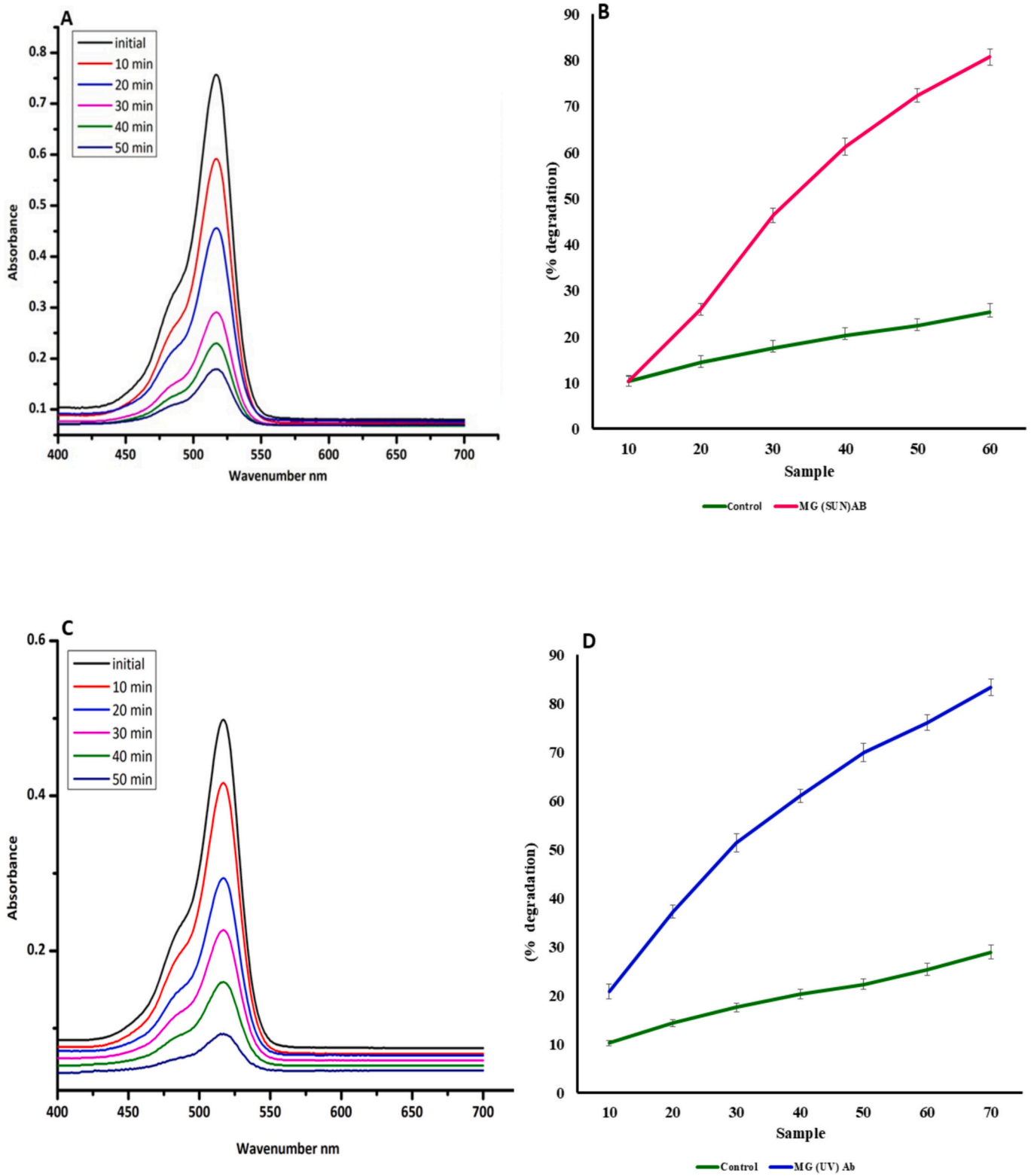

Fig. 3. Photocatalytic dye reduction (A) UV–visible spectra of Eosin Y dye under sunlight for *Ab* (B) % Degradation of Eosin Y dye under sunlight for *Ab* (C) UV–visible spectra of Eosin Y dye under sunlight for *GL* (D) % Degradation of Eosin Y dye under sunlight for *GL* (E) UV–visible spectra of Eosin Y dye under UV-light for *Ab* (F) % Degradation of Eosin Y dye under UV-light for *Ab* (G) UV–visible spectra of Eosin Y dye under UV for *GL* (H) % Degradation of Eosin Y dye under UV for *GL* (I) UV–visible spectra of Malachite green dye under sunlight for *Ab* (J) % Degradation of Malachite green dye under sunlight for *Ab* (K) UV–visible spectra of Malachite green dye under UV-light for *GL* (L) % Degradation of Malachite green dye under UV-light for *GL* (M) UV–visible spectra of Malachite green dye under sunlight for *GL* (N) % Degradation of Malachite green dye under sunlight for *GL* (O) UV–visible spectra of Malachite green dye under UV-light for *Ab* (P) % Degradation of Malachite green dye under UV-light for *Ab*. The results are expressed as mean (n = 3) ± standard deviation. (For interpretation of the references to color in this figure legend, the reader is referred to the web version of this article.)

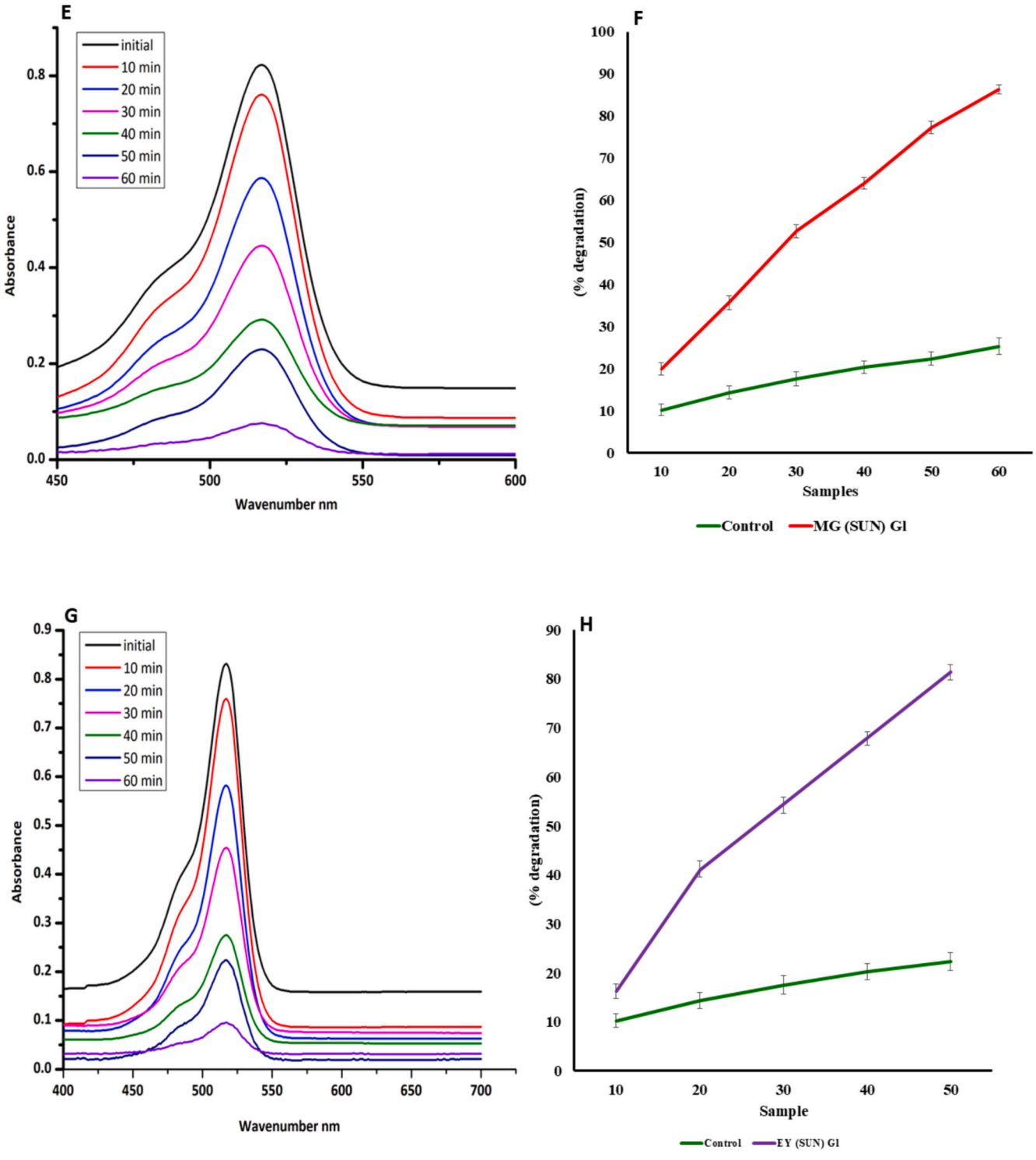

Fig. 3. (*continued*).

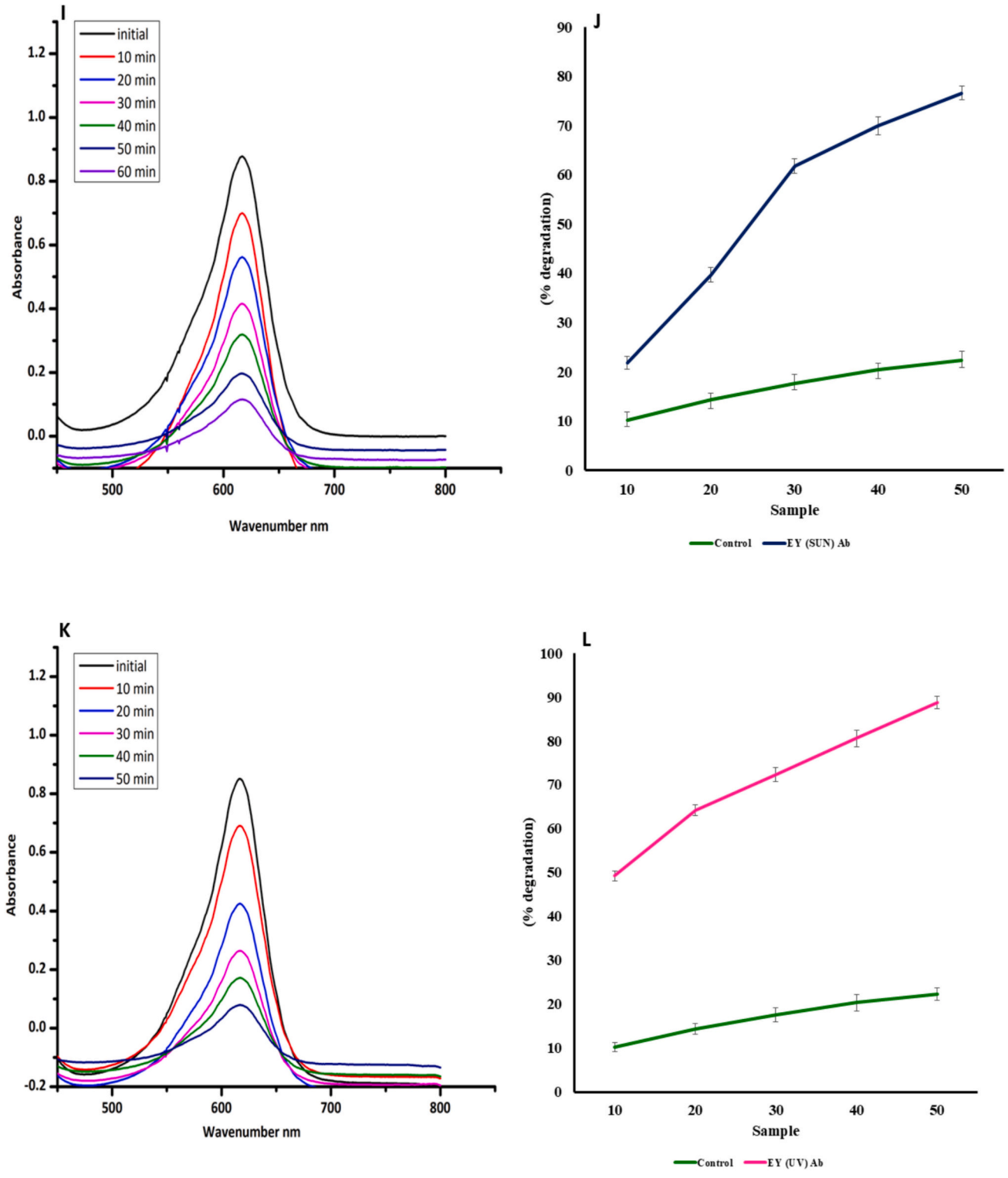

Fig. 3. (*continued*).

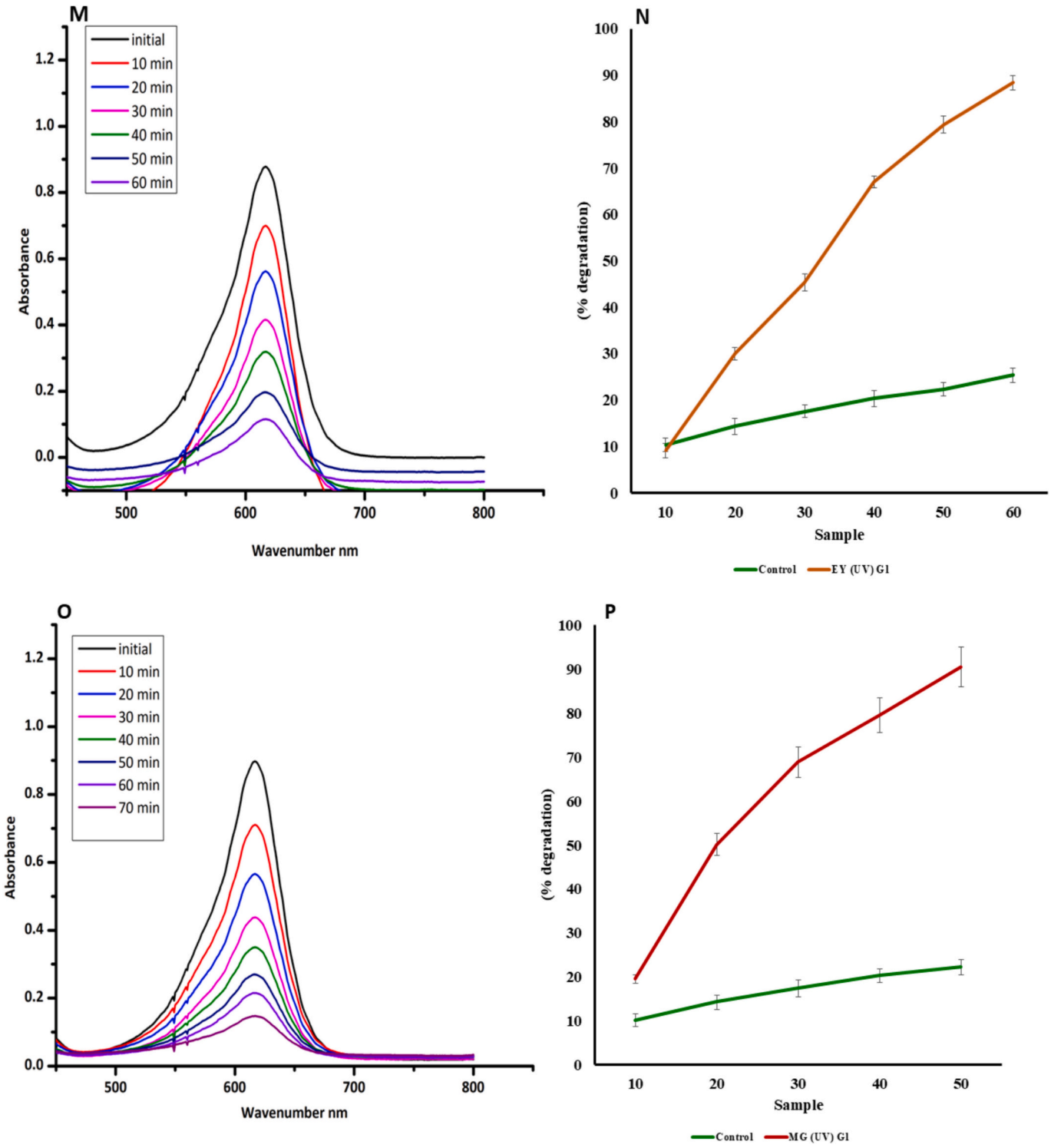

Fig. 3. (*continued*).

gradually release calcium, enhancing cellular retention. *A. bisporus*, with its different mineral-binding properties facilitates faster transport but less retention due to quicker release and absorption dynamics. These findings suggest that *G. lucidum* enhances zinc and calcium bioavailability due to superior retention mechanisms majorly facilitated by its unique polysaccharide content and fibrous structure, whereas *A. bisporus* improves iron status through higher retention potentially due to its protein and organic acid interactions. Combining both macro-fungi in the diet could optimize the bioavailability of these essential minerals which usually maximize the strengths of each species for improved overall mineral absorption and retention. The study of Kała et al. (2021) found the bioavailability of phenolic compounds and elements in various edible mushroom mycelia.

3.5.2. *Ferritin content*

The ferritin content was determined to observe the storage of iron in cells. The measurement of cellular uptake was measured as the ratio of ferritin to cell protein (ng ferritin/mg cell protein) and the results are

represented in Table 4. The present study demonstrates that there was a significant increase ($p < 0.05$) in the synthesis of ferritin in CaCo-2 cells upon exposure to *G. lucidum* and *A. bisporus* powder which showed a comparable factor related to their distinct biochemical compositions and mineral-binding properties. The study shows that *G. lucidum* significantly enhances ferritin synthesis (28.68 ± 0.62 ng ferritin/mg cell protein) as compared to *A. bisporus* (25.17 ± 0.52 ng ferritin/mg cell protein). This increased ferritin synthesis with *G. lucidum* is majorly due to its higher iron transport efficiency and the presence of bioactive components that facilitate iron storage within cells. Moreover, *G. lucidum* contains higher levels of polysaccharides and triterpenoids which may enhance iron solubility and bioavailability leading to more efficient cellular uptake and storage. These bioactive compounds can form complexes with iron aiding its transport across the cell membrane and its incorporation into ferritin, the primary intracellular iron storage protein. The higher overall cell protein content with *G. lucidum* (141.55 ± 0.56 mg) to that of *A. bisporus* (130.38 ± 0.49 mg) also suggests that *G. lucidum* may promote better overall cellular health and protein synthesis providing a conducive environment for increased ferritin production. While *A. bisporus* effective in enhancing iron uptake and storage may have different mineral-binding properties and less pronounced effects on cellular protein synthesis resulting in significantly lower ferritin levels. The proteins and organic acids in *A. bisporus* aid in iron transport and stabilization within cells but they may not enhance ferritin synthesis to the same extent as the components in *G. lucidum*. Additionally, the findings are supported by other studies such as Oyetayo et al. (2021) highlighting the nutrient content and antioxidant activity of fungi enriched with minerals like zinc and iron, emphasizing the role of specific bioactive compounds in enhancing mineral bioavailability and storage.

3.6. Photocatalytic dye degradation

The present comparative research has been done to explore the potential of two different mushroom species including *Agaricus bisporus* and *Ganoderma lucidum* to degrade harmful dyes namely Eosin Y and Malachite Green, which are widely used in industries like textiles and can be difficult to break down in natural environments. By analyzing the UV–Vis absorption spectrum by analyzing the UV–Vis absorption spectrum as shown in Figs. 3(A-O). The degradation efficiency of both macro-fungi significantly improves when exposed to UV–visible light. Under sunlight, *A. bisporus* demonstrated a strong ability to degrade Eosin Y by about 70–80 % and Malachite Green by 65–75 %. The results shown in Fig. 3B and J highlight the mushroom's natural capacity to reduce the presence of dye. Meanwhile, *G.lucidum* outperformed *A. bisporus* by achieving a 75–85 % degradation rate for Eosin Y (Fig. 3D) and a 70–80 % reduction for Malachite Green (Fig. 3N). The higher degradation percentages of *G. lucidum* suggest it might be more suited to degrade these dyes, even under natural light. Moreover, when the study was performed under UV–visible light, the degradation efficiency improved significantly *A. bisporus* degraded both Eosin Y and Malachite Green by about 80–90 % as shown in Fig. 3F and P, respectively. However, *G. lucidum* surpassed by degrading both dyes by 85–955 under UV–visible conditions (Fig. 3H and L). This marked improvement under UV–visible light can be attributed to the higher energy and more suitable wavelength of this light source, which is capable of better achieving the photocatalysts present in the macro-fungi. Several factors are attributed to the activity of *G. lucidum* as compared to *A. bisporus* in degrading these dyes as it contains a higher concentration of ligninolytic enzymes like laccases and peroxidases, which are highly effective at breaking down complex dye molecules. These enzymes provide *G. lucidum* with a biochemical edge, making it more efficient in attempting both Eosin Y and Malachite Green. In addition to enzyme concentration, *G. lucidum* leads to superior photocatalytic properties. It generates a higher quantity of reactive oxygen species (ROS) under UV–visible light, which plays a critical role in oxidative dye degradation. The physical characteristics of *G. lucidum* such as its larger surface area and higher porosity further enhance this process by providing more active sites for dye interaction. The study aligns with the findings by (Dias et al., 2022) studied the effect of *Cordyceps militaris* zinc oxide-based nanoparticles to degrade the hazardous dye methylene blue by about 97 % in the presence of UV–visible radiation.

4. Conclusion

In conclusion, macrofungi including *Agaricus bisporus* and *Ganoderma lucidum* exhibit considerable potential in diverse fields such as food technology, pharmaceuticals, environmental bioremediation, and sustainable materials science. The evaluation of in vitro mineral bioavailability and cellular mineral uptake of major nutrients like iron, zinc, and calcium from macrofungi powder has not only enhanced our understanding of their nutritional profile but also provided new insights into their role in human health. Both species are rich in bioactive compounds with therapeutic properties, positioning them as valuable ingredients in functional foods and nutraceuticals. Additionally, this study has expanded the scope of bioremediation by demonstrating the effective photocatalytic degradation of synthetic dyes such as Eosin Y and Malachite Green using powdered macro-fungi exposed to sunlight and UV irradiation. This novel application highlights the potential of these fungi in waste water purification and environmental detoxification, offering cost-effective and sustainable solutions for reducing industrial pollution and contributing to cleaner aquatic ecosystems. The study thus brings the gap between food technology and environmental sustainability, opening avenues for further research in bioremediation, nutraceuticals, and green technologies. By integrating the functional properties of macro-fungi into various industrial applications, the research contributes significantly to existing knowledge, offering innovative strategies for addressing global challenges in both health and environmental protection.

CRediT authorship contribution statement

Vaishali Singh: Writing – original draft, Methodology, Investigation, Formal analysis, Data curation. **Aarti Bains:** Writing – review & editing, Methodology, Investigation, Formal analysis. **Gulden Goksen:** Data curation, Methodology, Validation, Writing - review & editing. **Vittorio Capozzi:** Writing – review & editing, Methodology. **Anarase Dattatray Arjun:** Writing – review & editing, Methodology, Formal analysis. **Nemat Ali:** Writing – review & editing, Methodology, Funding acquisition. **Muzaffar Iqbal:** Writing – review & editing, Methodology. **Prince Chawla:** Writing – review & editing, Visualization, Validation, Supervision, Resources, Project administration, Methodology, Investigation, Conceptualization.

Declaration of competing interest

The authors declare that they have no known competing financial interests or personal relationships that could have appeared to influence the work reported in this paper.

Data availability

Data will be made available on request.

Acknowledgements

Support of Central Instrument Facility Lovely Professional University is greatfully acknowledged. Also, authors are thankful to the Researchers Supporting Project number (RSPD2024R734), King Saud University, Riyadh, Saudi Arabia for supporting this study

References

Abdulrauf, L. B., & Tan, G. H. (2016). Use of carbon nanotubes for the analysis of pesticide residues in fruits and vegetables. *Journal of AOAC International.*. https://doi.org/10.5740/jaoacint.16.0275

Akcay, C., Ceylan, F., & Arslan, R. (2023). Production of oyster mushroom (Pleurotus ostreatus) from some waste lignocellulosic materials and FTIR characterization of structural changes. *Scientific Reports, 13*(1). https://doi.org/10.1038/s41598-023-40200-x

Atik, A., Atik, İ., Akarca, G., & Denizkara, A. J. (2024). Incorporating Ganoderma lucidum extract and powder with probiotic cultures (*Lactobacillus acidophilus* and *Bifidobacterium animalis* subsp. lactis) enhanced the functional, textural, and sensory qualities of yogurt. *Journal of Food Science and Technology*. https://doi.org/10.1007/s13197-024-06068-z

Breene, W. M. (1990). Nutritional and medicinal value of specialty mushrooms. *Journal of Food Protection, 53*(10), 883–894.

Cao, Y., Zhang, M., & Chen, H. (2021a). Structural characterization and biological activity of polysaccharides from Ganoderma lucidum: Effect of different extraction methods. *International Journal of Biological Macromolecules, 166*, 766–774.

Cao, Y., Zhang, M., & Chen, H. (2021b). Structural characterization and biological activity of polysaccharides from Ganoderma lucidum: Effect of different extraction methods. *International Journal of Biological Macromolecules, 166*, 766–774.

De, S., Chawla, P., Dattatray, A., Iqbal, M., Goksen, G., Dhull, S. B., … Bains, A. (2024). Formulation of functional noodles by adding Lentinus edodes mushroom powder: Physiochemical attributes, cellular mineral uptake and improved glycemic index. *Food Chemistry: X, 101900*, Article 101900.

Demirtas, N., Sengul, G. F., Dizeci, N., & Yildirim, O. (2024). Exploring the chemical composition and nutritional properties of six edible mushroom species from Turkey. *Journal of Food Composition and Analysis, 133*, Article 106477.

Devi, P. V., Islam, J., Narzary, P., Sharma, D., & Sultana, F. (2024). Bioactive compounds, nutraceutical values and its application in food product development of oyster mushroom. *Journal of Future Foods, 4*(4), 335–342.

Dias, C., Ayyanar, M., Amalraj, S., Khanal, P., Subramaniyan, V., Das, S., Gandhale, P., Biswa, V., Ali, R., Gurav, N., Nadaf, S., Rarokar, N., & Gurav, S. (2022). Biogenic synthesis of zinc oxide nanoparticles using mushroom fungus Cordyceps militaris: Characterization and mechanistic insights of therapeutic investigation. *Journal of Drug Delivery Science and Technology, 73*(103444), Article 103444.

Du, X., Mu, H., Zhou, S., Xu, Z., & Yang, Y. (2018a). Morphological, structural, and physicochemical characterization of Agaricus bisporus powder. *Food Chemistry, 239*, 289–296.

Du, X., Mu, H., Zhou, S., Xu, Z., & Yang, Y. (2018b). Morphological, structural, and physicochemical characterization of Agaricus bisporus powder. *Food Chemistry, 239*, 289–296.

Fan, H.-B., Zou, Y., Huang, S.-Y., Liu, Y.-L., Zheng, Q.-W., Guo, L.-Q., & Lin, J.-F. (2021). Study on the physicochemical and emulsifying property of proteins extracted from Pleurotus tuoliensis. *Lebensmittel-Wissenschaft Und Technologie [Food Science and Technology], 151*(112185), Article 112185.

Gao, J., Li, X., Jia, S., Zeng, H., & Zheng, B. (2023). Structural characterization and antioxidant activity of a glycoprotein isolated from shiitake mushrooms. *Food Bioscience, 53*(102608), Article 102608.

Gao, Y., Chang, H., Liang, D., Yang, X.-Y., Chen, Z.-Q., & Liu, X. (2023). Harnessing *Prunella vulgaris* L. residues for enhanced biosorption of dyes in wastewater. *Chemical Engineering Research & Design: Transactions of the Institution of Chemical Engineers, 200*, 469–480.

Ghafoor, A., Rana, A., & Niazi, A. R. (2024). Systematic characterisation, mineral analysis, and valorisation of lignocellulosic waste into sustainable indigenous Ganoderma lucidum production from Pakistan. *New Zealand Journal of Botany*, 1–17.

Ghose, A., Nuzelu, V., Gupta, D., Kimoto, H., Takashima, S., Harlin, E. W., … Mitra, S. (2024). Micropollutants (ciprofloxacin and norfloxacin) remediation from wastewater through laccase derived from spent mushroom waste: Fate, toxicity, and degradation. *Journal of Environmental Management, 366*(121857), Article 121857.

Ghuniem, M. M., Gad, N., Tahon, M. A., & Ryad, L. (2024). Exposure assessment of pesticide residues, heavy metals, and veterinary drugs through consumption of Egyptian fish samples. *Toxicology Reports, 13*(101724), Article 101724.

Gong, P., Huang, Z., Guo, Y., Wang, X., Yue, S., Yang, W., Chen, F., Chang, X., & Chen, L. (2022a). The effect of superfine grinding on physicochemical properties of three kinds of mushroom powder. *Journal of Food Science, 87*(8), 3528–3541.

Gong, P., Huang, Z., Guo, Y., Wang, X., Yue, S., Yang, W., Chen, F., Chang, X., & Chen, L. (2022b). The effect of superfine grinding on physicochemical properties of three kinds of mushroom powder. *Journal of Food Science, 87*(8), 3528–3541.

Gong, P., Huang, Z., Guo, Y., Wang, X., Yue, S., Yang, W., Chen, F., Chang, X., & Chen, L. (2022c). The effect of superfine grinding on physicochemical properties of three kinds of mushroom powder. *Journal of Food Science, 87*(8), 3528–3541.

Guo, X., Zhu, K., Zhang, Y., & Zhang, X. (2021a). Physicochemical properties and thermal behavior of Ganoderma lucidum polysaccharides. *Carbohydrate Polymers, 254*. https://doi.org/10.1016/j.carbpol.2020.117353

Guo, X., Zhu, K., Zhang, Y., & Zhang, X. (2021b). Physicochemical properties and thermal behavior of Ganoderma lucidum polysaccharides. *Carbohydrate Polymers, 254*. https://doi.org/10.1016/j.carbpol.2020.117353

Haro, A., Trescastro, A., Lara, L., Fernández-Fígares, I., Nieto, R., & Seiquer, I. (2020a). Mineral elements content of wild growing edible mushrooms from the southeast of Spain. *Journal of Food Composition and Analysis: An Official Publication of the United Nations University, International Network of Food Data Systems, 91*(103504), Article 103504.

Haro, A., Trescastro, A., Lara, L., Fernández-Fígares, I., Nieto, R., & Seiquer, I. (2020b). Mineral elements content of wild growing edible mushrooms from the southeast of Spain. *Journal of Food Composition and Analysis: An Official Publication of the United Nations University, International Network of Food Data Systems, 91*(103504), Article 103504.

Haro, A., Trescastro, A., Lara, L., Fernández-Fígares, I., Nieto, R., & Seiquer, I. (2020c). Mineral elements content of wild growing edible mushrooms from the southeast of Spain. *Journal of Food Composition and Analysis: An Official Publication of the United Nations University, International Network of Food Data Systems, 91*(103504), Article 103504.

Hassan, F. R. H., El-Kader, A., & El-Sheikh, E. M. (2020a). Influence of drying methods on the physicochemical properties and mineral content of Agaricus bisporus. *Journal of Food Science and Technology, 57*(8), 2973–2981.

Hassan, F. R. H., El-Kader, A., & El-Sheikh, E. M. (2020b). Influence of drying methods on the physicochemical properties and mineral content of Agaricus bisporus. *Journal of Food Science and Technology, 57*(8), 2973–2981.

Hu, W., Di, Q., Liang, T., Zhou, N., Chen, H., Zeng, Z., Luo, Y., & Shaker, M. (2023). Effects of in vitro simulated digestion and fecal fermentation of polysaccharides from straw mushroom (Volvariella volvacea) on its physicochemical properties and human gut microbiota. *International Journal of Biological Macromolecules, 239* (124188), Article 124188.

Huang, W., Zhang, S., Zhang, M., & Zhang, P. (2019a). Structural characterization and immunomodulatory activity of polysaccharides from Ganoderma lucidum. *Carbohydrate Polymers, 205*, 192–199.

Huang, W., Zhang, S., Zhang, M., & Zhang, P. (2019b). Structural characterization and immunomodulatory activity of polysaccharides from Ganoderma lucidum. *Carbohydrate Polymers, 205*, 192–199.

Iqbal, T., Sohaib, M., Iqbal, S., & Rehman, H. (2024). Comprehensive nutritional profiling and antioxidant capacity assessment of indigenous mushrooms Pleurotus ostreatus and Agaricus bisporus. *Czech Journal of Food Sciences, 42*(3), 174–183.

Jin, M., Xie, Y., Xie, P., Zheng, Q., Wei, T., Guo, L., Lin, J., Ye, Z., & Zou, Y. (2022). Physicochemical and functional properties of Pleurotus geesteranus proteins. *Food Research International (Ottawa, Ont.), 162*(Pt A), Article 111978.

Kała, K., Krakowska, A., Szewczyk, A., Ostachowicz, B., Szczurek, K., Fijałkowska, A., & Muszyńska, B. (2021). Determining the amount of potentially bioavailable phenolic compounds and bioelements in edible mushroom mycelia of Agaricus bisporus, Cantharellus cibarius, and Lentinula edodes. *Food Chemistry, 352*(129456), Article 129456.

Kalač, P. (2016a). Edible mushrooms: Chemical composition and nutritional value. *Forest Products Journal, 66*(3–4), 216–222.

Kalač, P. (2016b). Edible mushrooms: Chemical composition and nutritional value. *Forest Products Journal, 66*(3–4), 216–222.

Khan, M. D., Singh, A., Khan, M. Z., Tabraiz, S., & Sheikh, J. (2023). Current perspectives, recent advancements, and efficiencies of various dye-containing wastewater treatment technologies. *Journal of Water Process Engineering, 53* (103579), Article 103579.

Kim, H., Kang, S., Li, K., Jung, D., Park, K., & Lee, J. (2021a). Preparation and characterization of various chitin-glucan complexes derived from white button mushroom using a deep eutectic solvent-based ecofriendly method. *International Journal of Biological Macromolecules, 169*, 122–129.

Kim, H., Kang, S., Li, K., Jung, D., Park, K., & Lee, J. (2021b). Preparation and characterization of various chitin-glucan complexes derived from white button mushroom using a deep eutectic solvent-based ecofriendly method. *International Journal of Biological Macromolecules, 169*, 122–129.

Kim, H., Kang, S., Li, K., Jung, D., Park, K., & Lee, J. (2021c). Preparation and characterization of various chitin-glucan complexes derived from white button mushroom using a deep eutectic solvent-based ecofriendly method. *International Journal of Biological Macromolecules, 169*, 122–129.

Lai, M. D., Chai, O. K., Arumugam, B., & Kuppusamy, U. R. (2024). Nutritional composition, efficacy and mechanisms of oyster mushrooms (Pleurotus spp.) in preventing metabolic syndrome: Insights into perspectives and challenges. *Food. Bioscience, 104768*.

Lavanya, K., Balagangadharan, K., Chandran, S. V., & Selvamurugan, N. (2023). Chitosan-coated and thymol-loaded polymeric semi-interpenetrating hydrogels: An effective platform for bioactive molecule delivery and bone regeneration in vivo. *Biomaterials Advances, 146*(213305), Article 213305.

Liang, S., Wang, X., Xie, L., Liu, X., & Dang, X. (2024). Discarded enoki mushroom root-derived multifunctional chrome-free chitosan-based tanning agent for eco-leathers manufacturing: Tanning-dyeing, non-acid soaking, and non-basifying. *International Journal of Biological Macromolecules, 275*(Pt 2), Article 133394.

Liu, X., Cao, Y., & Bai, C. (2018a). Characterization of polysaccharides from Ganoderma lucidum and their antioxidant activities through different thermal analysis methods. *Journal of Thermal Analysis and Calorimetry, 134*(3), 2145–2153.

Liu, X., Cao, Y., & Bai, C. (2018b). Characterization of polysaccharides from Ganoderma lucidum and their antioxidant activities through different thermal analysis methods. *Journal of Thermal Analysis and Calorimetry, 134*(3), 2145–2153.

Manimaran, K., Yanto, D. H. Y., Ardiati, F. C., Oktaviani, M., Natarajan, D., Ragavendran, C., … Loganathan, S. (2023). Enhanced photocatalytic degradation, antimicrobial and anticancer efficiency of mycosynthesized TiO2 nanoparticles using Pleurotus ostreatus mushroom extract: An eco-friendly approach. *Journal of Environmental Chemical Engineering, 111512*, Article 111512.

Mat Zin, M. I., Jimat, D. N., & Wan Nawawi, W. M. F. (2022). Physicochemical properties of fungal chitin nanopaper from shiitake (L. edodes), enoki (F. velutipes) and oyster mushrooms (P. ostreatus). *Carbohydrate Polymers, 281*(119038), Article 119038.

Mazumder, M. A. R., Jongraksang, K., Kaewsiri, K., Keawnualborvornnij, S., Nenjatee, W., Kaur, L., … Rawdkuen, S. (2024). Mushroom-legume-based alternative chicken nuggets: Physico-chemical and sensory properties. *Food Chemistry Advances, 5*(100777), Article 100777.

Mazumder, M. A. R., Sujintonniti, N., Chaum, P., Ketnawa, S., & Rawdkuen, S. (2023). Developments of plant-based emulsion-type sausage by using grey oyster mushrooms and chickpeas. *Foods (Basel, Switzerland), 12*(8), 1564.
Munir, S., Bozdar, H. B., & Memon, R. A. (2023). GC–MS, molecular identification, proximate and mineral content composition of two wild mushrooms (Ganoderma lucidum, Pleurotus ostreatus) from Gilgit Baltistan northern area of Pakistan. *Suid-Afrikaanse Tydskrif Vir Plantkunde [South African Journal of Botany], 163*, 57–64.
Nambafu, R., Waudo, J., Nganga, M., Lusi, P., & Nyambaka, H. (2023). Bioaccesibility of trace elements in different oyster mushroom varieties grown in Kenya. *Advances in Research, 24*(4), 29–37.
Oyetayo, V. O., Ogidi, C. O., Bayode, S. O., & Enikanselu, F. F. (2021). Evaluation of biological efficiency, nutrient contents and antioxidant activity of Pleurotus pulmonarius enriched with zinc and Iron. *Indian Phytopathology, 74*(4), 901–910.
Ozel, N., & Elibol, M. (2024). Chitin and chitosan from mushroom (Agaricus bisporus) using deep eutectic solvents. *International Journal of Biological Macromolecules, 262*, 130110.
Pandey, A., Pathak, V. M., Navneet, & Rajput, M. (2024). A feasible approach for azo-dye (methyl orange) degradation by textile effluent isolate *Serratia marcescens* ED1 strain for water sustainability: AST identification, degradation optimization and pathway hypothesis. *Heliyon, 10*(11), Article e32339.
Patil, N. D., Bains, A., Kaur, S., Yadav, R., Goksen, G., Ali, N., … Chawla, P. (2024). Effect of dual modifications with ultrasonication and succinylation on *Cicer arietinum* protein-iron complexes: Characterization, digestibility, in-vitro cellular mineral uptake and preparation of fortified smoothie. *Food Research International (Ottawa, Ont.), 186*, Article 114344.
Petre, M., & Teodorescu, T. I. (2020a). Influence of harvesting time and storage conditions on the quality and nutritional value of Agaricus bisporus. *Journal of Food Quality*. https://doi.org/10.1155/2020/8890476
Petre, M., & Teodorescu, T. I. (2020b). Influence of harvesting time and storage conditions on the quality and nutritional value of Agaricus bisporus. *Journal of Food Quality*. https://doi.org/10.1155/2020/8890476
Pratti, P. G., Junior, J. D. S. P., de Lima Petito, N., da Silva, B. D., Conte-Junior, C. A., Branco, V. N. C., … Domingues, J. R. (2024). Effect of hot air-drying and pasteurization on ergothioneine content in edible mushrooms. *Journal of Food Composition and Analysis, 126*, Article 105865.
Quero, J., Paesa, M., Morales, C., Mendoza, G., Osada, J., Teixeira, J. A., … Rodríguez-Yoldi, M. J. (2024). Biological properties of boletus edulis extract on Caco-2 cells: Antioxidant, anticancer, and anti-inflammatory effects. *Antioxidants (Basel, Switzerland), 13*(8), 908.
Reis, F. S., Martins, A., Barros, L., & Ferreira, I. C. F. R. (2017a). Chemical composition and nutritional value of Agaricus bisporus L.: White and brown mushrooms. *Food Chemistry, 230*, 396–403.
Reis, F. S., Martins, A., Barros, L., & Ferreira, I. C. F. R. (2017b). Chemical composition and nutritional value of Agaricus bisporus L.: White and brown mushrooms. *Food Chemistry, 230*, 396–403.
Saxami, G., Kerezoudi, E. N., Mitsou, E. K., Koutrotsios, G., Zervakis, G. I., Pletsa, V., & Kyriacou, A. (2021). Fermentation supernatants of Pleurotus eryngii mushroom ameliorate intestinal epithelial barrier dysfunction in lipopolysaccharide-induced Caco-2 cells via upregulation of tight junctions. *Microorganisms, 9*(10), 2071.
Sethi, S., Bharshankh, A., Sahu, R., & Biswas, R. (2024). Nano-bioremediation for sustainable treatment of waste: Applications, advancements, and challenges. In *Environmental engineering and waste management* (pp. 539–575). Springer Nature Switzerland.
Shahid-Ul-Islam, Bairagi, S., & Kamali, M. R. (2023). Review on green biomass-synthesized metallic nanoparticles and composites and their photocatalytic water purification applications: Progress and perspectives. *Chemical Engineering Journal Advances, 14*(100460), Article 100460.
Shams, R., Singh, J., Dash, K. K., & Dar, A. H. (2022). Comparative study of freeze drying and cabinet drying of button mushroom. *Applied Food Research, 2*(1), Article 100084.
Sharma, M., Bains, A., Sridhar, K., Chawla, P., & Sharma, M. (2023). Process optimization for spray dried *Aegle marmelos* fruit nanomucilage: Characterization, functional properties, and in vitro antibiofilm activity against food pathogenic microorganisms. *International Journal of Biological Macromolecules, 249*(126050), Article 126050.
de Souza, D. F., da Silva, M., De, C. S., de Souza, T. C., Rocha, G. C., Kasuya, M. C. M., & Eller, M. R. (2023). Effect of selenium-enriched substrate on the chemical composition, mineral bioavailability, and yield of edible mushrooms. *Biological Trace Element Research, 201*(6), 3077–3087.
Smith, D. F., Dragotakes, Q., Kulkarni, M., Hardwick, J. M., & Casadevall, A. (2022). Galleria mellonella immune melanization is fungicidal during infection. *Communications Biology, 5*(1), 1364.
Tang, J., Yao, D., Xia, S., Cheong, L., & Tu, M. (2024). Recent progress in plant-based proteins: From extraction and modification methods to applications in the food industry. *Food Chemistry: X, 23*(101540), Article 101540.
Tang, Y., Yu, H., & Shen, W. (2021). Effects of drying methods on physicochemical properties and bioactivities of Ganoderma lucidum. *Food Chemistry, 340*. https://doi.org/10.1016/j.foodchem.2020.127933
Teli, S. A., Seikh, A. Y., Shukla, R. M., Richa, R., Faisal, S., Kumar, S., … Kumar, A. P. (2024). Numerical optimization of drying of white button mushroom (Agaricus bisporus) employing microwave and fluidized bed drying for preparing value added product. *Journal of Agriculture and Food Research, 101360*.
Tian, Y., Zhang, D., Cai, D., Liu, H., & Liu, G. (2019a). Influence of drying methods on physicochemical properties and antioxidant activities of Agaricus bisporus powder. *Food Science and Biotechnology, 28*(4), 1273–1281.
Tian, Y., Zhang, D., Cai, D., Liu, H., & Liu, G. (2019b). Influence of drying methods on physicochemical properties and antioxidant activities of Agaricus bisporus powder. *Food Science and Biotechnology, 28*(4), 1273–1281.
Tsai, S.-Y., Huang, F.-K., Juan, H.-W., & Lin, C.-P. (2018). Evaluation of food-processing conditions of various particle sizes of Tremella fuciformis powder via DSC and TG analyses. *Journal of Thermal Analysis and Calorimetry, 134*(2), 857–864.
Valverde, M. E., Hernández-Pérez, T., & Paredes-López, O. (2015a). Edible mushrooms: Improving human health and promoting quality life. *International Journal of Microbiology, 2015*, Article 376387.
Valverde, M. E., Hernández-Pérez, T., & Paredes-López, O. (2015b). Edible mushrooms: Improving human health and promoting quality life. *International Journal of Microbiology, 2015*, Article 376387.
Vélez-Uribe, T., Orozco-Agudelo, N., Manjarrés-Pinzón, G., Manjarrés-Pinzón, K., Gil-González, J., & Rodríguez-Sandoval, E. (2023). Physicochemical, antioxidant, and technofunctional properties of mushroom (Pleurotus sp) flour obtained by hot air drying. *Dyna, 90*(225), 85–94.
Wang, S., Qi, J., Cai, X., Wu, W., Wang, Z. A., Jiao, S., … Yang, Z. (2024). Advancements and future perspectives in the study of oligosaccharides derived from edible-medicinal mushrooms. *Food. Bioscience, 104874*.
Wickramasinghe, M. A., Nadeeshani, H., Sewwandi, S. M., Rathnayake, I., Kananke, T. C., & Liyanage, R. (2023). Comparison of nutritional composition, bioactivities, and FTIR-ATR microstructural properties of commercially grown four mushroom species in Sri Lanka; Agaricus bisporus, Pleurotus ostreatus, Calocybe sp. (MK-white), Ganoderma lucidum. *Food Production, Processing and Nutrition, 5*(1), 43.
Yang, J. H., Wang, Y., & Yu, J. H. (2019a). Physicochemical properties and antioxidant activities of Ganoderma lucidum spore powder after heat and ultrasound treatments. *Journal of Food Science and Technology, 56*(7), 3363–3372.
Yang, J. H., Wang, Y., & Yu, J. H. (2019b). Physicochemical properties and antioxidant activities of Ganoderma lucidum spore powder after heat and ultrasound treatments. *Journal of Food Science and Technology, 56*(7), 3363–3372.
Yılmaz, F. M., & Zungur Bastıoğlu, A. (2020). Production of phenolic enriched mushroom powder as affected by impregnation method and air drying temperature. *Lebensmittel-Wissenschaft Und Technologie [Food Science and Technology], 122*(109036), Article 109036.
Ying, Z., Han, X., & Li, J. (2019a). Thermal stability and degradation kinetics of Agaricus bisporus polysaccharides. *International Journal of Biological Macromolecules, 140*, 1125–1132.
Ying, Z., Han, X., & Li, J. (2019b). Thermal stability and degradation kinetics of Agaricus bisporus polysaccharides. *International Journal of Biological Macromolecules, 140*, 1125–1132.
Yusran, Y., Erniwati, E., Khumaidi, A., Pitopang, R., & Jati, I. R. A. P. (2023). Diversity of substrate type, ethnomycology, mineral composition, proximate, and phytochemical compounds of the Schizopyllum commune Fr. In the area along Palu-Koro Fault, Central Sulawesi, Indonesia. *Saudi Journal of Biological Sciences, 30*(4), Article 103593.
Zhang, J., Yagoub, A. E. A., Sun, Y., Arun, M. S., Ma, H., & Zhou, C. (2022). Role of thermal and non-thermal drying techniques on drying kinetics and the physicochemical properties of shiitake mushroom. *Journal of the Science of Food and Agriculture, 102*(1), 214–222.
Zhang, Y., Zhu, J., Zou, Y., Ye, Z., Guo, L., & Zheng, Q. (2024). Insoluble dietary fiber from five commercially cultivated edible mushrooms: Structural, physiochemical and functional properties. *Food Bioscience, 57*(103514), Article 103514.
Zheng, L., Sun, Y., Liu, S., Wei, Y., & Zhang, W. (2020a). Thermal properties and antioxidant activities of polysaccharides extracted from Agaricus bisporus. *Journal of Thermal Analysis and Calorimetry, 139*(5), 3067–3076.
Zheng, L., Sun, Y., Liu, S., Wei, Y., & Zhang, W. (2020b). Thermal properties and antioxidant activities of polysaccharides extracted from Agaricus bisporus. *Journal of Thermal Analysis and Calorimetry, 139*(5), 3067–3076.

Further-reading

Li, J. F., Rupa, E. J., Hurh, J., Huo, Y., Chen, L., Han, Y., … Yang, D.-C. (2019a). Cordyceps militaris fungus mediated zinc oxide nanoparticles for the photocatalytic degradation of methylene blue dye. *Optik, 183*, 691–697.
Li, J. F., Rupa, E. J., Hurh, J., Huo, Y., Chen, L., Han, Y., … Yang, D.-C. (2019b). Cordyceps militaris fungus mediated zinc oxide nanoparticles for the photocatalytic degradation of methylene blue dye. *Optik, 183*, 691–697.
Rahman, M. A., Al Masud, A., Lira, N. Y., & Shakil, S. (2020). Proximate analysis, phtochemical screening and antioxidant activity of different strains of Ganoderma lucidum (Reishi mushroom). *Open Journal of Biological Sciences, 5*(1), 024–027.
Rijia, A., Krishnamoorthi, R., Rasmi, M., Mahalingam, P. U., & Kim, K. S. (2024). Comprehensive analysis of bioactive compounds in wild Ganoderma applanatum mushroom from Kerala, South India: Insights into dietary nutritional, mineral, antimicrobial, and antioxidant activities. *Pharmaceuticals, 17*(4), 509.
Zhang, H. L., Wei, J. K., Wang, Q. H., Yang, R., Gao, X. J., Sang, Y. X., … Chen, Q. J. (2019). Lignocellulose utilization and bacterial communities of millet straw based mushroom (Agaricus bisporus) production. *Scientific Reports, 9*(1), 1151.